Downloaded from orbit.dtu.dk on: Apr 17, 2024

DTU Library

Deoxygenation of wheat straw fast pyrolysis vapors over Na-Al_2O_3 catalyst for production of bio-oil with low acidity

Eschenbacher, Andreas; Saraeian, Alireza; Jensen, Peter Arendt; Shanks, Brent H.; Li, Chengxin; Duus, Jens Øllgaard; Smitshuysen, Thomas Erik Lyck; Damsgaard, Christian Danvad; Hansen, Asger Baltzer; Kling, Kirsten Inga

Total number of authors:
14

Published in:
Chemical Engineering Journal

Link to article, DOI:
10.1016/j.cej.2020.124878

Publication date:
2020

Document Version
Peer reviewed version

Link back to DTU Orbit

Citation (APA):
Eschenbacher, A., Saraeian, A., Jensen, P. A., Shanks, B. H., Li, C., Duus, J. Ø., Smitshuysen, T. E. L., Damsgaard, C. D., Hansen, A. B., Kling, K. I., Mentzel, U. V., Henriksen, U. B., Ahrenfeldt, J., & Jensen, A. D. (2020). Deoxygenation of wheat straw fast pyrolysis vapors over Na-Al_2O_3 catalyst for production of bio-oil with low acidity. *Chemical Engineering Journal*, *394*, Article 124878. https://doi.org/10.1016/j.cej.2020.124878

General rights
Copyright and moral rights for the publications made accessible in the public portal are retained by the authors and/or other copyright owners and it is a condition of accessing publications that users recognise and abide by the legal requirements associated with these rights.

- Users may download and print one copy of any publication from the public portal for the purpose of private study or research.
- You may not further distribute the material or use it for any profit-making activity or commercial gain
- You may freely distribute the URL identifying the publication in the public portal

If you believe that this document breaches copyright please contact us providing details, and we will remove access to the work immediately and investigate your claim.

Deoxygenation of wheat straw fast pyrolysis vapors over Na-Al_2O_3 catalyst for production of bio-oil with low acidity

Andreas Eschenbacher[a], Alireza Saraeian[b], Peter Arendt Jensen[a], Brent H. Shanks[b], Chengxin Li[c], Jens Øllgaard Duus[c], Thomas Erik Lyck Smitshuysen[d], Christian Danvad Damsgaard[d, e], Asger Baltzer Hansen[f], Kirsten Inga Kling[e], Uffe Vie Mentzel[f], Ulrik Birk Henriksen[a], Jesper Ahrenfeldt[a], Anker Degn Jensen[a,*]

[a]Department of Chemical and Biochemical Engineering, Technical University of Denmark, 2800 Kgs. Lyngby, Denmark

[b]Department of Chemical and Biological Engineering, Iowa State University, Ames, IA 50011, United States

[c]Department of Chemistry, Technical University of Denmark, 2800 Kgs. Lyngby, Denmark

[d]Department of Physics, Technical University of Denmark, 2800 Kgs. Lyngby, Denmark

[e]National Centre for Nano Fabrication and Characterization, Technical University of Denmark, 2800 Kgs. Lyngby

[f]Haldor Topsøe A/S, 2800 Kgs. Lyngby, Denmark

KEYWORDS. Wheat Straw; Sodium; Alumina; Micro-Pyrolyzer; Catalytic Fast Pyrolysis; TAN; ^{13}C NMR

ABSTRACT

Catalytic upgrading of pyrolysis vapors from wheat straw over Na_2CO_3 impregnated γ-Al_2O_3 was studied as a promising route to biofuels. The Na species were homogenously distributed on the support and created a basicity of ~0.02 mmol CO_2/g catalyst, at 80% lower catalyst acidity. Analytical pyrolysis using a micro-pyrolyzer showed that Na-Al_2O_3 particularly decreased the yield of acids via ketonization, which was confirmed by feeding carboxylic acid model compounds. The presence of Na decreased the coke yield and catalyzed the coke combustion, decreasing the combustion temperature by ~100 °C.

Subsequently, 100 g Na-Al_2O_3 catalyst was tested in an ablative bench scale fast pyrolysis unit where ~5 kg of wheat straw was pyrolyzed and the vapors passed the catalytic reactor during six reaction/regeneration cycles. In agreement with the micro-pyrolyzer results, Na-Al_2O_3 was highly effective in reducing the acidity of the bio-oils. Total acid numbers (TAN) as low as ~1-4 mg KOH/mg could be maintained up to high B:C ratios of ~13. For a given TAN, this allowed operating to higher B:C ratios and provided higher oil yields compared to using acidic catalysts such as γ-Al_2O_3 and HZSM-5 zeolite for vapor treatment. At bio-oil energy recoveries of ~60-70% relative to raw bio-oil, the deoxygenation was comparable to the acidic catalysts. Operation to higher B:C ratios allowed increasing the energy recovery to ~85% relative to the non-treated bio-oil while still obtaining a good deoxygenation performance of ~60%. Despite the hydrothermal conditions during reaction and oxidative regeneration, the activity of Na-Al_2O_3 was regained by coke combustion, the Na remained well dispersed on the support, and the catalyst maintained its capacity for CO_2 adsorption at 500 °C after six reaction/regeneration cycles.

1 INTRODUCTION

Fast pyrolysis (FP) processes are generally flexible with respect to biomass feedstocks [1–8]. The integration of biomass-derived FP oils in existing oil refineries may allow to decrease our

dependence on crude oil and increase the share of renewables in the transport sector [9–12]. Unfortunately, the pyrolysis oil contains hundreds of different oxygenated species, which render the oil acidic and unstable. The acidity of untreated bio-oil causes severe corrosion in commercial operation [13] and separate feed lines and tanks with stainless steel cladding would be necessary for bio-oil processing in order to minimize corrosion [14,15].

The fuel properties and miscibility with fossil feedstock can be improved via catalytic deoxygenation of the biomass pyrolysis vapors prior to condensation [12,16–24]. However, these improvements come at the expense of carbon loss as light hydrocarbons, CO, CO_2, and coke [25,26]. Amongst the variety of catalysts tested for pyrolysis vapor up-grading (without hydrogen addition), microporous HZSM-5 zeolite is considered a suitable solid acid catalyst for the production of aromatics and gasoline range products from biomass derived pyrolysis vapors [27,28]. Nevertheless, rapid deactivation by coking occurs [18,29]. Beside other zeolites [30–33], acidic oxides like silica-alumina and γ-Al_2O_3 have been found active for deoxygenation of FP vapors [34–38]. In addition, basic oxides like ZnO and MgO are claimed to have good deoxygenation activity [39–43].

The first use of Na_2CO_3 for production of upgraded pyrolysis oil was reported by Babich et al. [44], who impregnated chlorella algae with Na_2CO_3 solution and pyrolyzed the modified algae (20 wt.% Na_2CO_3) at different temperatures. Although the oxygen content was not measured, towards increased pyrolysis temperature (450 °C), a similar energy recovery of the catalytic FP oil was obtained compared to the non-catalytic reference (~40%), while a clear decrease in (especially small) acids was observed by GC-MS, along with an increase in pH from 2.7 to 3.5.

In continuation of Babich et al.'s work [44], a high activity of alkali modified amorphous silica-alumina and alumina catalysts was reported for deoxygenation of pyrolysis vapors derived from

66 woody biomass [45–48]. Using a laboratory packed-bed pyrolysis unit, Zabeti et al. [48] found 10
67 wt.% Na on amorphous silica alumina effective for deoxygenation of pinewood pyrolysis vapors.
68 However, no significant changes in the content of carboxylic acids detected by GC-MS was
69 reported. For a Na-based faujasite zeolite on the other hand, it was reported that acids and
70 aldehydes/ketones were effectively removed [49]. Nguyen et al. [50] reported the deoxygenation
71 of pine pyrolysis vapors using a packed-bed system as described in reference [48] over 20 wt.%
72 Na_2CO_3/γ-Al_2O_3 at a biomass-to-catalyst ratio (B:C) of 2. While a severe drop in oil yield was
73 observed from 41 wt.% to 9 wt.% and the yield of coke from biomass was 15 wt.%, the oxygen
74 content (d.b.) and TAN of the oil decreased from 42 wt.% O and 119 mg KOH/g to 12 wt.% O
75 and 4 mg KOH/g, respectively. In a later work, Nguyen et al. [51] tested different Na_2CO_3 loadings
76 on an alumina support. FP vapors from sugarcane bagasse were generated in a fluidized-bed
77 reactor (100 g/h feeding rate) and upgraded over a fixed bed of 20 g catalyst. Unfortunately, the
78 final cumulative B:C ratio was not reported but the optimum performance was obtained using 25
79 wt.% Na_2CO_3. The deoxygenation activity of the 25 wt.% Na_2CO_3/γ-Al_2O_3 catalyst was found
80 comparable to HZSM-5 (Si/Al ~ 15), albeit the Na-Al_2O_3 catalyst showed a higher coke yield (4.1
81 wt.%) compared to HZSM-5 (2.3 wt.%) and a lower yield of organic fraction (26.2 wt.% vs. 27.8
82 wt.%).

83 Xue et al. [52] tested five kinds of sodium salts (carbonate, silicate, aluminate, sulfate, and
84 chloride) supported on γ-Al_2O_3 for the upgrading of pine pyrolysis vapors generated in a horizontal
85 fixed-bed reactor (2 g biomass and 1 g catalyst). All salts effectively removed acids. The oxygen
86 content was most effectively reduced when using Na_2CO_3 and Na_2SiO_2 for the impregnation. The
87 γ-Al_2O_3-supported Na_2SiO_2 catalyst was suggested as the best performing candidate since it
88 obtained a slightly higher oil yield compared to the other γ-Al_2O_3-supported Na salts. However,

89 the O/C ratio was slightly higher for the oil obtained using the Na_2SiO_2 impregnated catalyst
90 compared to Na_2CO_3 impregnation and as such the benefit appears ambiguous.
91 To the best of our knowledge, to date the stability of Na-Al_2O_3 catalysts has only been addressed
92 for a single regeneration [45]. While Na content and textural properties were reported to remain
93 stable, upgrading of FP vapors over the regenerated catalyst produced bio-oil with a higher oxygen
94 content (~20 wt.%) compared to oil obtained over the fresh catalyst (12 wt.%). This was attributed
95 to a change in the active hydrated sodium species during regeneration.
96 In this work, the stability of the Na-Al_2O_3 catalyst was studied for extended
97 reaction/regeneration cycles in a continuous FP set-up. Compared to earlier reported oil
98 characterization by GC-MS, elemental composition, heating value and TAN, we conducted
99 additional oil characterization by one- and two-dimensional ^{13}C and ^{1}H NMR, GCxGC, basic
100 nitrogen determination, and thermogravimetric analysis in order to fully determine the chemical
101 composition and fuel properties of the oils derived from wheat straw FP vapors after catalytic
102 treatment with Na-Al_2O_3. In addition, we addressed the following research questions:
103 i) What yields and oil quality can be obtained from deoxygenation of wheat straw FP vapors
104 using a Na_2CO_3/Al_2O_3 catalyst in a continuous bench unit?
105 ii) How is the oil yield and quality influenced by increased processing of FP vapors (i.e.
106 increasing B:C)?
107 iii) How does the performance of a Na_2CO_3/Al_2O_3 catalyst compare to frequently used acidic
108 catalysts such as γ-Al_2O_3, HZSM-5, mesoporous HZSM-5, and HZSM-5/γ-Al_2O_3?
109 These aspects need to be addressed in order to determine the frequency of regeneration needed
110 to maintain a certain bio-oil quality in a parallel vapor-upgrading fixed bed scenario [53]. The

111 results obtained using the bench scale system were complemented by catalytic studies in a
112 micro-scale reactor and a comparison between these two systems was attempted.

113 2 MATERIAL AND METHODS

114 2.1 Feedstock

115 The biomass feedstock was obtained by downsizing wheat straw pellets using a hammer mill.
116 For the bench scale investigations, a sieve fraction <1.4 mm was used, while for the micro-
117 pyrolysis (μ-Py) a sieve fraction of 106–250 μm was used. The respective ultimate and proximate
118 characterization for the two different sieve fractions are shown in Table 1. More details about the
119 analysis methods of the feedstock can be found in references [18] and [54]. While the two fractions
120 showed a comparable elemental composition on dry and ash-free basis (daf), the finer sieve
121 fraction contained a higher amount of ash.

122 **Table 1.** Properties of wheat straw used in micro and bench scale experiments.

Proximate analysis	wheat straw (0–1.4 mm) used for bench scale tests	wheat straw (0.1–0.25 mm) used for μ-Py tests
Moisture (as received (a.r.)), wt.%	8.8	7.1
Volatiles (dry basis, (d.b.) wt.%	66.8	74.4
Fixed carbon (d.b., by diff.) wt.%	18.5	15.8
Ash (d.b.) wt.%	5.9	9.8
Elemental composition (dry and ash-free basis (daf))		
Nitrogen wt.%	0.8	1.3
Carbon wt.%	50.4	48.2
Hydrogen wt.%	5.6	5.0
Sulfur wt.%	0.1	0.1
Oxygen (by diff.) wt.%	43.1	45.4

123

124 2.2 Catalyst preparation

125 Extrudates of γ-Al_2O_3 were provided by Haldor Topsøe A/S and downsized prior to wet
126 impregnation in excess water. For the addition of 20 wt.% Na_2CO_3, one part of Na salt was
127 dissolved in water, after which four parts of γ-Al_2O_3 was added. The slurry was stirred overnight,
128 poured in glass trays and dried in an oven at 105 °C. The catalyst was downsized to a range of 36–

125 μm for the tests with the μ-Py, while a larger sieve fraction of 250–850 μm was used in the bench scale reactor. Prior to reaction, the catalyst was calcined in a muffle furnace under ambient air. The temperature was increased by 5 °C/min to 550 °C and the final temperature was held for 5 h. Note that the catalyst used for the μ-Py and bench scale tests was prepared in two separate batches.

2.3 Catalyst characterization

The Na content was determined by XRF. The method was described in detail in our earlier work [18]. The Na distribution of the fresh and regenerated (after six reaction/regeneration cycles) catalysts was studied by scanning electron microscopy-energy dispersive X-ray spectroscopy (SEM-EDS). Samples were ground and sieved to <50 μm before adding them on a copper grid with lacey carbon film. A FEI Nova 600 NanoSEM equipped with a FlatQuad (Bruker, USA) EDS detector was used to image the particles and measure their elemental composition by mapping the entire imaged area. The microscope was operated in high vacuum at 6 kV acceleration voltage and a beam current of 0.62 nA. The sample was mounted at 10 mm working distance below the polepiece and approximately 4 mm under the annular FlatQuad detector. Particles were imaged with the Everhardt Thornley secondary electron detector at a magnification of 40000x and maps were acquired with a pixel dwelltime of 16 μs and image resolution of 800 pixels in X for a couple of minutes, to achieve a statistically significant number of counts (>10000).

N_2 physisorption was carried out on a Quantachrome Novatouch apparatus at liquid nitrogen temperature. Prior to the measurement, samples were outgassed under vacuum at 350 °C overnight. The specific surface area (S_{BET}) was calculated by the Brunauer-Emmett-Teller (BET) method in the relative pressure range of 0.05 to 0.3. The total pore volume (V_{total}) was calculated from the amount of adsorbed nitrogen at the relative pressure of $p/p_0 = 0.99$. The Barrett-Joyner-Halenda

(BJH) pore size distribution was derived from the adsorption branch of the N_2 physisorption isotherm for calculation of the volume and surface area of mesopores (20–500 Å pore width).

Temperature programmed desorption (TPD) of ammonia (NH_3) and CO_2 was used for characterization of the acid and base sites on the catalysts, respectively. The measurements were performed using a Micromeritics Autochem II 2920 Chemisorption Analyzer. Samples were pre-treated at 500 °C (heating ramp: 10 °C/min) in 25 mL/min He for 1 h. The sample was then cooled to 100 °C and NH_3 was adsorbed for 120 min (20 mL/min of 1 vol% NH_3 in He) followed by a flowing He purge for 60 min. The NH_3 desorption while heating the samples to 500 °C using a 5 °C/min ramp in 25 mL/min He was recorded by a thermal conductivity detector (TCD). For the basic site measurement, samples were pre-treated at 500 °C (heating ramp: 10 °C/min) in 25 mL/min He for 1 h. The sample was then cooled to 50 °C and 100% CO_2 was adsorbed for 30 min (50 mL/min) followed by purging the sample with He for 60 min. Under the same flow conditions, the CO_2 desorption during heating at 10 °C/min to 500 °C was recorded by TCD. NH_3-TPD and CO_2-TPD curves were normalized based on the sample mass.

In order to investigate any differences in the CO_2 chemisorption capacity under operating conditions (500 °C), TPD-MS tests were performed using an Autosorb iQ instrument (3P instruments) which was coupled to a Hiden QGA gas analyzer. 1 g of catalyst that was stored under ambient air conditions was packed in a U-shaped quartz reactor in between plugs of quartz wool. Under Helium flow (~40 Nml/min), the sample temperature was increased to 110 °C and held for 2 h in order to remove moisture. Then, the sample temperature was increased to 600 °C at 10 °C/min in helium flow and any evolving CO_2 (m/z = 44) was monitored with the MS. After heating to 600 °C, the sample temperature was lowered to 500 °C in helium flow, and the gas was switched to 100% CO_2. After purging with CO_2 for 30 min, the gas was changed to helium again.

After flushing with helium for 90 min, the temperature was again increased to 600 °C at 10 °C/min while monitoring evolved CO_2.

The weight change of the catalyst during heating was investigated using a thermogravimetric analyzer (Netzsch STA 449 F1 Jupiter ASC). About 50 mg of catalyst was loaded in an alumina crucible, and the temperature was increased at 10 °C/min until reaching 900 °C while maintaining a flow of 100 ml/min N_2.

The crystalline phases of the samples were examined by powder X-ray diffraction (Empyrean from Malvern Analytical). The catalyst samples were crushed and sieved <50 μm before being pressed into pellets for analysis. The incident beam was generated using a Cu-anode of wavelength 1.5418 Å (Empyrean Cu LFF HR). The diffracted beam was filtered through a monochromator and detected (PIXcel3D-Medipix3). During acquisition, samples were spun with 3.75 rotations/min and the 2θ-angles was scanned from 7° to 60° in 0.0131° steps.

A calcined Na-Al_2O_3 sample from the 100 g batch tested at bench scale and a spent catalyst sample that was recovered after six reaction-regeneration cycles was further investigated by in situ XRD and quadrupole mass spectrometry (QMS). The powder sample was loaded on a ceramic holder and mounted into a furnace with X-ray transparent beryllium windows (XRK 900, Anton Paar) situated within an X'pert Pro diffractometer (Malvern Panalytical) with a $Cu_{K\alpha}$-anode. The diffracted beam was filtered through a monochromator. The sample was heated step-wise with one hour long XRD-measurements (2θ range 13 to 42°), at 110 °C, 250 °C, 350 °C and 600 °C in He flow (100 ml/min) at 1 bar. Subsequently the sample was cooled to 500 °C and kept for two hours with a flow of CO_2 (74 ml/min) at 1 bar before changing back to He for 3 hours. Finally, it was heated to 600°C in He for two hours. The gas-exhaust was monitored using QMS supplied by Pfeiffer.

2.4 Pyrolysis units

Sections 2.4.1 and 2.4.2 summarize the experimental conditions applied in the μ-Py and the bench scale system. The two scales should not be compared quantitatively, only qualitatively, since they operate at very different ratios of flow rate to catalyst mass. In addition, the bench-Py determines yields from condensed product while the μ-Py uses GC for vapor quantification, which will therefore mainly determine the lighter components.

2.4.1 Micro-pyrolyzer (μ-Py) setup

The μ-Py study was carried out using a single-shot tandem micro-pyrolysis system (Rx-3050tr, Frontier Labs, Japan) and the formed vapors were analyzed by a GC-MS/FID/TCD (see Fig. S1) using He as carrier gas at a flow rate of 60 mL/min and a split ratio of 1:56. A detailed description of the experimental set-up and experimental conditions of this study can be found in the work of Nolte et al. [55] and Eschenbacher et al. [54]. The top pyrolysis reactor and the bottom catalytic reactor were maintained at 530 °C and 500 °C, respectively. 0.59 ±0.01 mg of wheat straw was loaded into stainless steel sample cups and the cups (16 in total) were introduced into the pyrolysis reactor via an autosampler. The catalytic reactor contained a quartz tube loaded with a mixture of 60 mg quartz beads (150–215 μm, acid washed and calcined at 550 °C) and the catalyst (2 mg, 36–125 μm). The catalyst bed was secured between two quartz wool plugs and placed within the temperature-controlled isothermal zone of the tandem-reactor. After the reaction of 16 pyrolysis vapor pulses over the catalyst, the catalyst was regenerated by placing the quartz tube containing the catalyst into a muffle furnace and calcining the catalyst for 5 h at 550 °C (heating ramp 10 °C/min). A repetition experiment processing another 16 pyrolysis vapor pulses was performed with the regenerated catalyst.

For product analysis, the GC (Agilent 7890B) separation was completed using an initial oven temperature of 35 °C for 7.5 min followed by ramping at 10 °C/min to 300 °C. Condensable species

were separated using a medium polarity 1701 column (Agilent VF-1701 ms), identified by MS (Agilent 5977A), and quantified using FID based on calibration and molecular response factors (MRF), as elaborated in earlier work [54]. The products identified by FID were grouped into aliphatics (ALI), monoaromatics (MAR), di-aromatics (DAR), phenols (PH), aldehydes (ALD), acids (AC), ketones (KET), methoxy-phenols (MPH), furans (FUR), alcohols (ALC), and nitrogen containing compounds (N). Table S1-S11 provide an overview of the compounds contained in each product group along with their respective MRF.

The light gases were separated using a GasPro column (Agilent GS-GasPro) and quantified using TCD. To test the repeatability of the product analysis, three biomass injections were performed replacing the catalyst with 2 mg of SiC as highly inert material. Table S12 lists the individual product standard deviations based on these three repeated injections. The char yields were determined gravimetrically by weighing the sample cups and biomass before and after FP in the µ-Py. Coke yields were determined by combustion of the coke in a TGA (Netzsch STA449 F1) coupled with an MS (QMS 403 D Aëolos®), following the procedure described in Eschenbacher et al. [54].

2.4.2 Bench scale pyrolyzer

A description of the bench scale pyrolysis unit (bench-Py) can be found in earlier work [18], and a flow sheet is provided in Fig. S2. For this study, the flowrate of nitrogen carrier was set to 8.3 Nl/min and the temperature of the pyrolysis section, cyclone section, hot gas filter, and catalyst bed was set to 530 °C, 450 °C, 350 °C, and 500 °C, respectively. Biomass was fed into the pyrolysis zone at ~3.5 g/min until a desired cumulative biomass-to-catalyst weight ratio (B:C) was reached. For the regeneration of the catalyst, it was first cooled down to ~150 °C in N_2 flow before replacing the flow with 2 vol.% O_2/N_2 and heating the bed to 550 °C at 1 °C/min. The final temperature was held for several hours before the nitrogen was stepwise replaced by increasing amounts of air. The

regeneration was assumed complete once no CO and CO_2 were observed in the effluent gas stream. In total, six tests were performed (labeled A-F), and the catalyst was regenerated in between each test. Condensation was achieved by a three-stage condensation system consisting of i) a cold water bath at 4 °C, ii) an ESP for collection of aerosols generated during the initial quench, and iii) a series of impingers immersed in a dry-ice/EtOH bath at -60 °C. The dry gas was analyzed continuously for CO and CO_2 by nondispersive infrared and O_2 by paramagnetism and every ~10 min a sample was analyzed by GC-FID/TCD for analysis of C_1-C_6 hydrocarbons and H_2.

2.5 Oil characterization

The liquid products collected at the bench scale pyrolysis unit were kept refrigerated at 5 °C in order to minimize aging. For all tests, the condensed liquid product immediately phase-separated in an organic rich oil-phase—referred to as bio-oil within this study—and an aqueous phase.

Karl−Fischer titration, elemental analysis, and GC-MS/FID was conducted for the oil and aqueous fractions according to the details described elsewhere [18]. The oil phase was further analyzed for total acid number (TAN) following ASTM D664, and the basic nitrogen content of the oil was analyzed following UOP Method 269-10.

It is important to provide information on the charring behavior of the liquid products for comparison with literature and to assess how suited the bio-oils are for further processing [26]. In line with others [56,57], the evaporation behavior of the oils was studied by thermogravimetric analysis (TGA). About 20 mg of oil was loaded into a Pt crucible with lid shortly before start of the heating ramp in order to minimize the loss of volatiles. The temperature was ramped to 550 °C at 10 °C/min under N_2 atmosphere (150 ml/min). The revaporization efficiency was defined based on the mass% of the loaded (water-free) bio-oil that was volatilized at 350 °C.

A non-catalytic bio-oil and bio-oil that was obtained from vapor upgrading over a four times used and regenerated Na-Al_2O_3 catalyst at B:C ~4 was further characterized by GC×GC-ToF/MS

or−FID using a LECO® Pegasus 4DTM instrument. The instrument type and experimental conditions are described in more detailed in other work [SE-ART-12-2019-001254]. The NIST2008 mass spectral database was used of identification, and for quantification of different product groups, the FID was used. The compounds were classified into 13 groups: aliphatics (paraffins/naphthenes), monoaromatics (alkylbenzenes/naphthenobenzenes), di/tri-aromatics, carboxylic acids, pyrroles/nitriles, pentanones/hexanones, furanones/furfuryl alcohols, aliphatic ketone/other aliphatic oxygenates, indanones/benzofurans/dibenzofuranes, phenols/methoxybenzenes, methoxy-phenols, hydroxylated di/tri-aromatics, and dihydroxylated benzenes. The relative amount (FID area-%) of each compound class was estimated as the sum of areas of all detected peaks in that class divided by the total peak area of all compound classes.

^{1}H, ^{13}C NMR and 2D HSQC NMR analysis was performed for selected bio-oils. Details of the used instruments and experimental conditions are provided in earlier work [18]. The quantitative ^{13}C integration was performed following the procedure suggested by Ben and Ragauskas [58], while taking into account the modifications suggested by Happs et al. [59].

3 RESULTS

3.1 Catalyst properties

Isotherms and pore distribution from nitrogen physisorption are shown in Fig. S3. Note that the pores are in mesopore range (Fig. S3b) and as such the total pore volume and surface area are the same as the surface area and pore volume of mesopores. The Na impregnation decreased the pore volume and surface area from ~0.5 cc/g and >200 m^2/g to 0.34 cc/g and 125 m^2/g (see **Table 2**). A further decrease in pore volume and surface area was observed at the end of the bench-Py test series to ~0.28 cc/g and 100 m^2/g. The Na addition to γ-Al_2O_3 decreased the pore volume of pores with pore width < 200Å while slightly more pores with pore volume >200 Å were formed (see

293 Fig. S3). Due to the small amount of catalyst used with the μ-Py, no post-reaction characterization
294 was attempted.

295 The NH_3-TPD and CO_2-TPD results for the catalysts that were prepared and tested at bench
296 scale are shown in Fig. 1, while the characterization by NH_3-TPD for the catalysts tested at micro-
297 scale is provided in Fig. S4. The impregnation with Na_2CO_3 severely reduced the number of acid
298 sites (by ~80%), with only very weak (desorption at 100-200 °C) and medium (desorption at 200-
299 400 °C) acid sites remaining (see Fig. 1a). The calcination in dry air at 550 °C increased the acidity
300 only slightly for the dried Na-Al_2O_3. After six reaction-regeneration cycles at bench-scale, the
301 concentration of acids sites with weak to medium strength (desorption at 100-300 °C) increased
302 from 0.06 mmol/g to 0.11 mmol/g. At the same time, many basic sites with weak to medium
303 strength have been lost during the reaction-regeneration cycles, and only strong basic sites
304 (desorbing CO_2 between 250-500 °C) remained (Fig. 1b).

305 As such, it appears that over the course of the catalytic testing, basic (Na) species transformed
306 into other species, possibly facilitated by the reducing conditions and steam present under reaction
307 conditions.

308 The catalyst characterization by TGA is shown in Fig. S5. The main weight loss for the γ-Al_2O_3
309 support occurred at ~95 °C, attributed to atmospheric moisture, and the mass continued to decrease
310 at a lower rate with increasing temperature, which is attributed to phase changes accompanied by
311 dehydration [60–62]. The impregnated and dried Na-Al_2O_3 catalyst on the other hand shows four
312 more decomposition peaks at ~250 °C, ~325 °C, ~710 °C, and ~870 °C, which can be attributed
313 to the decomposition of different Na_2CO_3 species on the γ-Al_2O_3 surface. After calcination of the
314 catalyst, the intensity of the weight losses at ~250 °C, ~325 °C, and ~710 °C had decreased
315 appreciably, while the feature at ~870 °C remained the same. After three reaction/regeneration

316 cycles, the observed features for the dried, and the dried and calcined samples had disappeared
317 completely and the weight loss resembled more closely the TGA of the γ-Al_2O_3 support, i.e. only
318 dehydration. Thus, the TGA analysis is in agreement with the observed changes in CO_2-TPD. We
319 note that the calcined Na-Al_2O_3 catalyst desorbed CO_2 at ~250 °C, at which also a weight loss was
320 observed in TGA (Fig. S5). It is worth mentioning that the difference in weight loss between γ-
321 Al_2O_3 and dried Na-Al_2O_3 in the temperature range of 400-700 °C roughly agrees with a calculated
322 mass loss of 8.3% for the decomposition of Na_2CO_3 into Na_2O and CO_2. The difference between
323 calcined Na-Al_2O_3 and γ-Al_2O_3 was lower (4-6 mass%), and after multiple reaction/regeneration
324 cycles the difference in weight loss between the Na-Al_2O_3 and γ-Al_2O_3 was only 1-2%, which is
325 attributed to differences in moisture content. Nguyen et al. [46] had reported a difference in weight
326 loss between γ-Al_2O_3 and calcined Na-Al_2O_3 of 8.4 mass%. Both CO_2 and water were observed
327 during the weight loss, which suggested that the Na on the calcined catalyst was present as a
328 hydrated carbonate phase, raising the question if Na_2CO_3 is completely decomposed into Na_2O
329 and CO_2 during calcination at 550 °C and to what extent (and how rapid) Na_2O may take up
330 moisture and CO_2 from ambient air.
331 Assuming that the impregnated Na_2CO_3 decomposes to Na_2O and CO_2 during calcination, a
332 theoretical Na load of 9.5 wt.% is calculated. The elemental analysis by XRF determined Na
333 loadings of 9.1 wt.% and 9.6 wt.% for the catalysts prepared for the μ-Py tests and bench scale
334 tests, respectively, which is in good agreement with the theoretical loading. We note a discrepancy
335 to the Na content reported for 20 wt.% Na_2CO_3/γ-Al_2O_3 in the work by Nguyen et al. [45], since
336 the Na content in their case was reported as ~4.5 wt.%.
337

Table 2. Physicochemical characterization of γ-Al_2O_3, and Na impregnated γ-Al_2O_3 tested in the μ-Py. Textural parameters were derived from nitrogen adsorption data. Acidity and basicity was determined by temperature programed desorption of ammonia and CO_2, respectively. Numbers in brackets indicate values that were determined after six reaction/regeneration cycles.

	γ-Al_2O_3	Na-Al_2O_3 (μ-Py)	Na-Al_2O_3 (bench-Py)
V_{total} at p/p_0 =0.99	0.56 (0.49)	0.38	0.34 (0.28)
BET area [m^2/g]	268 (212)	113	125 (100)
Acidity [mmol NH_3/g]	0.30 (0.31)	0.06	0.06 (0.11)
Basicity [mmol CO_2/g]	0.004	0.021	0.018 (0.002)

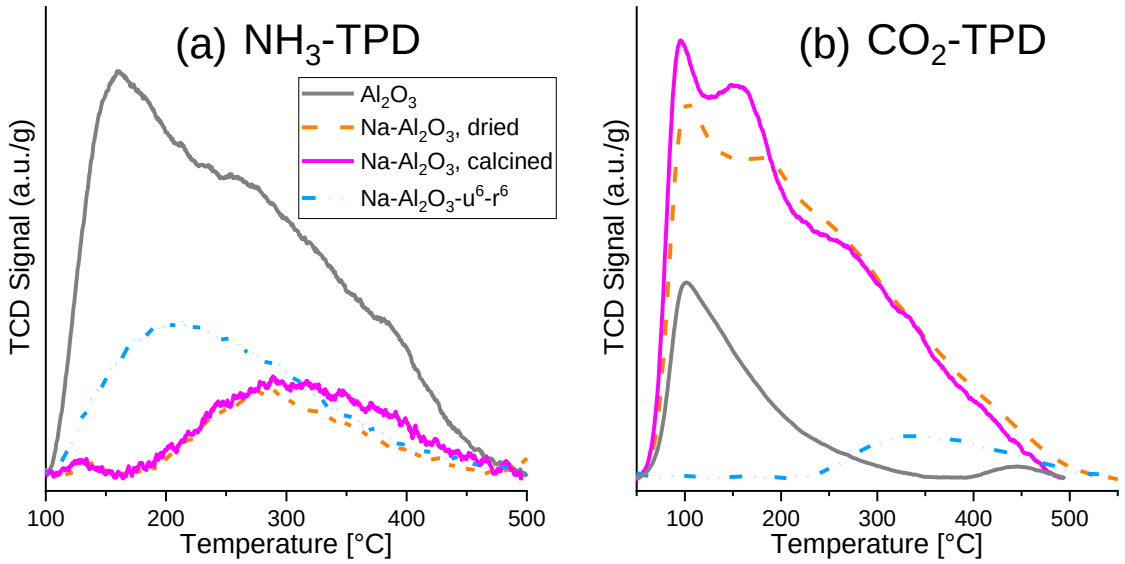

Fig. 1. (a) Temperature programmed desorption (TPD) of ammonia for parent γ-Al_2O_3 (black) and Na_2CO_3 impregnated γ-Al_2O_3 after impregnation and drying (red), calcination (blue), and six reaction/regeneration cycles (green). (b) TPD of CO_2. The legend in Fig. 1a also applies for Fig. 1b.

The XRD analysis (Fig. S6) shows that compared to the background pattern of the γ-Al_2O_3 support, additional peaks arise for the calcined Na-Al_2O_3 catalyst (prior to catalytic tests). The majority of the additional Bragg reflections correspond to Na_2CO_3 and hydrated Na_2CO_3, suggesting that the catalyst re-adsorbed CO_2 and H_2O after calcination.

3.2 Product distribution – μ-Py

Table S13 shows the structure of the 34 most prevalent compounds that were identified in the FP vapors generated in the μ-Py system. All compounds contain at least one oxygen functionality.

Aldehydes (ALD), ketones (KET), and furanic (FUR) compounds were the most prevalent compound types, followed by esters (EST) and methoxyphenols (MPH). Phenols (PH) and MPH are attributed to the decomposition of the lignin component of wheat straw, while anhydrosugars and smaller oxygenates result from the pyrolysis of hemicellulose and cellulose [63–65]. For the catalytic vapor upgrading, the change in product distribution was monitored for each biomass injection. Then, the integral yields at a certain cumulative weight ratio of injected biomass (daf) to loaded catalyst (2 mg) were calculated. For a series of 16 biomass injections of ~0.5 mg wheat straw (daf) per injection, a cumulative B:C ratio of ~4 was reached. Fig. S7 shows a comparison for the first and 16th biomass injection when using γ-Al_2O_3 as a catalyst. Fewer species were observed in the chromatogram for the first injection compared to the 16th injection, especially the compounds with higher MW eluting after ~17.5 min. This observation is in line with an effective cracking of the pyrolysis vapors. For the first injection, the vapors contain a few simple oxygenates (FUR and KET) with one oxygen functionality and simple aromatics. Due to catalyst deactivation, the 16th injection (B:C = 3.6–3.9) shows a large number of highly oxygenated compounds containing at least two oxygen atoms such as acids, esters, methoxy-phenols, and di-ketones, which are also observed when replacing the catalyst with a highly inert SiC (Fig. S7).

Compared to γ-Al_2O_3, Na-Al_2O_3 yielded less aromatics and more ketones (e.g. acetone and cyclopentenones) from the first biomass injection (Fig. S8). This can be explained by a decreased activity for catalytic cracking due to the reduced acidity compared to γ-Al_2O_3. Na-Al_2O_3 showed an increased activity for ketonization, which is the conversion of two organic acids to a ketone while oxygen is removed in the form of water and CO_2 [66–70]. Since CO_2 is one of the reaction products, it may poison strong base sites and make them unavailable for ketonization reaction. As the CO_2-TPD showed (Fig. 1b), even after repeated reaction/regeneration cycles some base sites

remained that desorb CO_2 below the reaction temperature (500 °C), which should thus be available for ketonization in the presence of CO_2. The ketonization reaction is beneficial as the formed ketones can be further converted to produce longer-chain hydrocarbons via aldol condensation/hydrogenation [71,72]. An increased concentration of di-methylated cyclopentenones and long chain compounds such as 2-heptadecanone observed in the Na-Al_2O_3 treated vapors suggests the occurrence of coupling reactions. When comparing the chromatograms for the 16th biomass injection obtained with γ-Al_2O_3 and Na-Al_2O_3, it becomes clear that in contrast to Al_2O_3, Na-Al_2O_3 was still active in converting acids and showed higher concentrations of certain ketones, e.g. (methyl-) pentanedione and butanedione.

Fig. 2 shows the carbon yields of the different product groups for each biomass injection as a function of increasing B:C. For γ-Al_2O_3, a rapid breakthrough of acids, ketones and aldehydes is observed which reach a constant yield at B:C ~2. The yield of methoxyphenols on the other hand continued to increase as B:C increased. For Na-Al_2O_3, the yield of ketones is high and stable from the beginning. The yield of ALD remained lower compared to γ-Al_2O_3 and most noticeable, the conversion of acids and methoxyphenols improved for the Na modified γ-Al_2O_3.

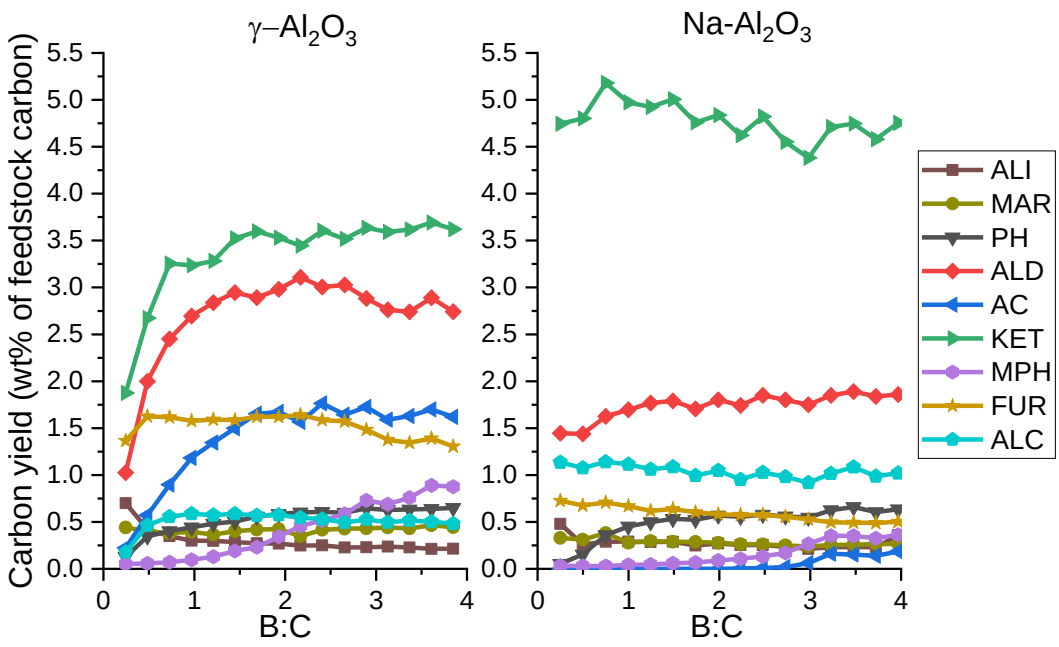

393

394 **Fig. 2**. Carbon yields of the different product groups. The abbreviations in the legend refer to aliphatics
395 (ALI), monoaromatics (MAR), phenols (PH), aldehydes (ALD), acids (AC), ketones (KET), methoxy-
396 phenols (MPH), furans (FUR) and alcohols (ALC).

397 Table 3 summarizes the (cumulative) product yields of vapors, gas, and coke at B:C ~4. The
398 char yield was 18.3 wt.% (±0.08) of fed wheat straw (daf), which is in agreement with char yields
399 of 18-21 wt.% (daf) obtained for the same feedstock and pyrolysis temperature at the bench scale
400 FP unit [18,19,73]. Higher gas yields were attained for Na-Al_2O_3 compared to γ-Al_2O_3 . The coke
401 yield was 1.5 wt.% of fed biomass for Na-Al_2O_3 while it was 2.7 wt.% for Al_2O_3, which explains
402 why Al_2O_3 deactivates more rapidly than Na-Al_2O_3 as observed from the differences between the
403 16th injections of the two catalysts (see Fig. S7 and S8). Lower yields of ALD, AC, MPH, and
404 FUR and higher yields of KET and ALC were obtained for the Na-Al_2O_3 compared to γ-Al_2O_3. It
405 is worth pointing out that the overall yield of compounds with ketone functionalities was highest
406 in the non-catalytic case (**Table 3**). To discern the ketonization activity, the ketone product group
407 was further divided into two subgroups:

i) ketones with multiple oxygen functionalities such as hydroxy-ketones, di-ketones, and cyclopentenone- and cyclopentanone –derivatives with two or more oxygen functionalities, and

ii) linear ketones and cyclopentenone- and cyclopentanone –derivatives with a single oxygen functionality.

A full list of the compounds contained in the two ketone subgroups is provided in Table S14. The ketones observed in the non-catalytic case are predominantly contained in group i), but some acetone and cyclopentenone is already present in the non-catalytic vapors, which were grouped as group ii) ketones. Cyclopentenones originate from the decomposition of carbohydrates in the biomass [74] and the presence of alkalines such potassium during fast pyrolysis can further enhance these minor carbohydrate-derived products [75]. The ketones with single oxygen functionality, especially linear ketones, are considered ketonization products. This subdivision shows that both γ-Al_2O_3 and Na-Al_2O_3 decreased the yield of highly oxygenated group i) ketones at a cumulative B:C of ~4, as shown in Table S15. While no increase in the yield of group ii) ketones was observed for γ-Al_2O_3, the yield of simple ketones increased from 1.4 wt% for the blank test (SiC) to 2.4 wt% when using Na-Al_2O_3, which in combination with the effective conversion of acids is a strong indication for ketonization.

Evidence for the ketonization activity of Na-Al_2O_3 was obtained by feeding acetic acid, propionic acid, and a 50/50 vol% mix of the two acids over Na-Al_2O_3 at 500 °C. As seen by the FID chromatograms in Fig. S9, acetone was the main product when feeding acetic acid, 3-pentanone was the main product when feeding propionic acid, and 2-butanone was the main product of the mixture while about the same amount of acetone and 3-pentanone were also produced. Ketonization of acetic acid with propionic acid thus gives 2-butanone, while at the same

time self-condensation of acetic acid (yielding acetone) and self-condensation of propionic acid (yielding 3-pentanone) take place.

Table 3. Product yields (wt.% of fed biomass (daf)) at B:C ~4. Results obtained with SiC as a highly inert solid shown for reference. Vapors, gas, and coke were quantified by GC-FID, GC-TCD, and TGA, respectively. Char yield was 18.3 wt.% (±0.08) for all tests.

	vapors									gas					coke
	ALI	MAR	PH	ALD	AC	KET	MPH	FUR	ALC	CO	CO_2	C_{1-3}	$C_{2-3=}$	C_4+	
SiC	0.1	0.0	0.3	1.8	2.4	3.9	0.9	0.9	0.7	7.1	17.1	0.1	0.3	0.3	~0
γ-Al_2O_3	0.2	0.2	0.3	2.3	1.7	2.6	0.3	1.1	0.6	8.4	17.2	0.1	0.6	0.6	2.7
Na-Al_2O_3	0.1	0.2	0.3	1.5	0.3	3.5	0.3	0.4	0.9	10.3	18.0	0.0	1.3	1.0	n.d.
Na-Al_2O_3 (after single use and regenerated)	0.2	0.1	0.3	1.5	0.1	3.5	0.1	0.4	1.2	9.5	18.0	0.1	1.1	0.9	1.5

The elemental composition of the char from the μ-Py was assumed to be the same as determined in bench scale; namely 80 wt.% C, 4 wt.% H, 2 wt.% N, and 14 wt.% O (by difference) on a daf basis. Thus, the carbon recovery of char was ~31 wt.% for all tests. The carbon closure (**Table 4**) was ~61 wt.% for the non-catalytic case, while it was improved slightly to ~63-66% when using a catalyst due to the increased carbon recoveries of gas, vapors and coke. The missing carbon is attributed to i) non-identified compounds in the FID chromatogram and ii) deposits of oligomeric species with highly reactive functionalities that may polymerize and deposit at the interface between the reactors (300 °C), the GC-inlet (270 °C), and the guard column inlet [54]. Larger scale catalytic experiments, discussed under section 3.3, are thus indispensable for the assessment of the elemental composition and quality of the bio-oil. Nevertheless, the differences in deactivation, based on the breakthrough of primary pyrolysis vapors and differences in products can be compared for different catalysts using the micropyrolyzer. **Table 4** summarizes the obtained product carbon recoveries. For γ-Al_2O_3, the cumulative C recovery of the vapors at B:C ~4 was 11.5%, which is close to SiC and can be explained by the rapid deactivation of the catalyst. For

Na-Al_2O_3 the carbon recovery of vapors was lower (9.4%), which can be attributed to the elevated gas yields. As indicators for the fuel properties upon condensation of the vapors, **Table 4** lists the wt.% acidity, the oxygen content, the higher heating value (HHV), and the effective hydrogen index (EHI) for the vapors. The oxygen content and the acidity of the GC-identified vapors was calculated as

$wt.\%\ O = \frac{\text{mass of oxygen in vapors}}{\text{mass of vapors}}$, and

$acidity = \frac{\text{yield of acids in vapors}}{\text{mass yield of vapors}}$.

The EHI is a calculated indicator of the 'net' H/C ratio of a feed after debiting the feed's hydrogen content for complete conversion of heteroatoms to NH_3, H_2S, and H_2O according to

$EHI = \frac{H-2O-3N-2S}{C}$ [76].

Overall, Na-Al_2O_3 produced vapors with highly reduced acidity and moderate deoxygenation (due to ketonization). The heating value of the accumulated vapors at B:C ~4 improved from 24.6 MJ/kg for the non-catalytic SiC to 27.0 MJ/kg and ~29 MJ/kg when γ-Al_2O_3 and Na-Al_2O_3 was used as a catalyst, respectively. For γ-Al_2O_3 and Na-Al_2O_3 the HHV of the treated vapors decreased from 30.1 and 29.8 MJ/kg to 26.3 and 29.1 MJ/kg for the first and 16th vapor pulse, respectively.

Favorably, EHI >1 was obtained with Na-Al_2O_3, which is expected to reduce the coking propensity upon further processing of the condensed oil by fluid catalytic cracking (FCC). The performance of the Na-Al_2O_3 after a single oxidative regeneration cycle was comparable to its initial use (**Table 4**, Fig. S10), and the yield of the identified acids (acetic and propionic acid) was even lower for the regenerated catalyst (0.04 wt.% of fed biomass) compared to its initial use (0.29 wt.%).

Table 4. Carbon balance and vapor properties. For SiC, the vapor properties were determined from three biomass injections. For vapor treatment with γ-Al_2O_3 and Na-Al_2O_3, the properties are reported for the accumulated vapors of 16 biomass injections corresponding to B:C ~4.

	Carbon recovery			Cumulative vapor properties			
	C-% vapors	C-% gas	C-% coke	Acidity vapors (wt.%)	wt.% O vapors	HHV* of vapors [MJ/kg]	EHI† vapors
SiC	12.6	17.3	~0	22.1	37.1	24.6	0.67
γ-Al_2O_3	11.5	19.9	4.3	17.6	32.6	27.0	0.88
Na-Al_2O_3	9.4	21.8	n.d.	3.6	30.0	28.7	1.01
Na-Al_2O_3 (after single use and regenerated)	9.4	20.3	3.1	0.7	28.9	29.4	1.06

*calculated based on CHNO content of vapors according to correlation reported by Channiwala and Parikh [77].
†calculated based on definition by Chen et al. [76].

3.3 Product distribution – bench scale pyrolysis unit

Six tests were performed using the bench scale FP unit denoted by A-F in chronological order. Tests A, B, and C were performed to investigate the change in oil yield and energy recovery towards increasing biomass to catalyst ratio (up to B:C = 12.7). Tests D and E were performed to test the catalyst stability, since test A, D, E were all stopped at B:C ~4. Finally, test F was performed to repeat the operation to high B:C > 10. **Fig. 2** shows the obtained product yields with respect to the fed biomass and includes two non-catalytic references obtained with an empty catalytic reactor or ~100 g SiC. The mass balance closure was in the range 92-97% (standard deviation 1.7%), and the missing mass is attributed to char accumulations in the system, and volatilization prior to weighing of the condensation equipment. The inline catalytic treatment with Na-Al_2O_3 only slightly increased the dehydration and decarbonylation, while a pronounced increase in decarboxylation was observed with 7.6-10.7 percentage point higher CO_2 yields compared to the empty reactor reference (**Fig. 2**). This is in agreement with observations by Nguyen et al. [46] who noted an increase in CO_2 yields from 5 to 12 wt.%. A decrease in the molar CO/CO_2 ratio from 0.66 to 0.60 was also observed in this study using the μ-Py.

Upon contact of the catalyst (at operating temperature) with the FP vapors, the bed temperature increased by ~30 °C due to exothermic reactions after which the temperature slowly decreased (see Fig. S11). Significantly higher hydrogen concentrations in the gas resulted when using Na-Al_2O_3 compared to γ-Al_2O_3. The initially high CO_2 and H_2 concentration in the gas continued to decrease with time-on-stream, while the concentration of CO increased (see Fig. S11). The yields of H_2, CO, and CO_2 for the first use Na-Al_2O_3 (run A) was 0.6, 8.6, and 22.1 wt.%, respectively, while for repetitions D and E, the yield of H_2, CO, and CO_2 was 0.3, 9.1, and 20.5 wt.%, respectively. For comparison, the yield of H_2, CO, and CO_2 when using γ-Al_2O_3 as catalyst was 0.15, 9.8, and 13.7 wt.%, respectively. The lower CO and higher CO_2 and H_2 yields compared to γ-Al_2O_3 catalyst could indicate water gas shift (WGS) activity of the Na-Al_2O_3 catalyst, which is in line with an observed promoter effect of Na for WGS activity [78,79].

It is further noteworthy that the coking propensity of the Na-Al_2O_3 catalyst decreased after multiple reaction/regeneration cycles. This can be seen by comparing the coke yields of run A, D, E at B:C ~4 and will be discussed in more detail in section 3.5. At the same time, the yield of liquid range organics increased, while the O content of the liquid surprisingly did not increase, as discussed more in sections 3.4 and 3.7.

The non-catalytic reference of SiC and empty reactor show lower gas yields and higher yields of oil phase, but also much higher losses of organics to the aqueous phase, which is often considered wastewater. The yield (relative to fed biomass), of the aqueous phase, its water content, carbon concentration, and the carbon recovery with respect to fed biomass carbon in aqueous phase are summarized in Table S16. The water content and carbon content of the aqueous phase was 68 wt.% and 16 wt.% for the empty-reactor case, while for the catalytic runs the water content

increased above 92 wt% and the carbon content of the aqueous phase decreased to 3-5 wt% (see Table S16).

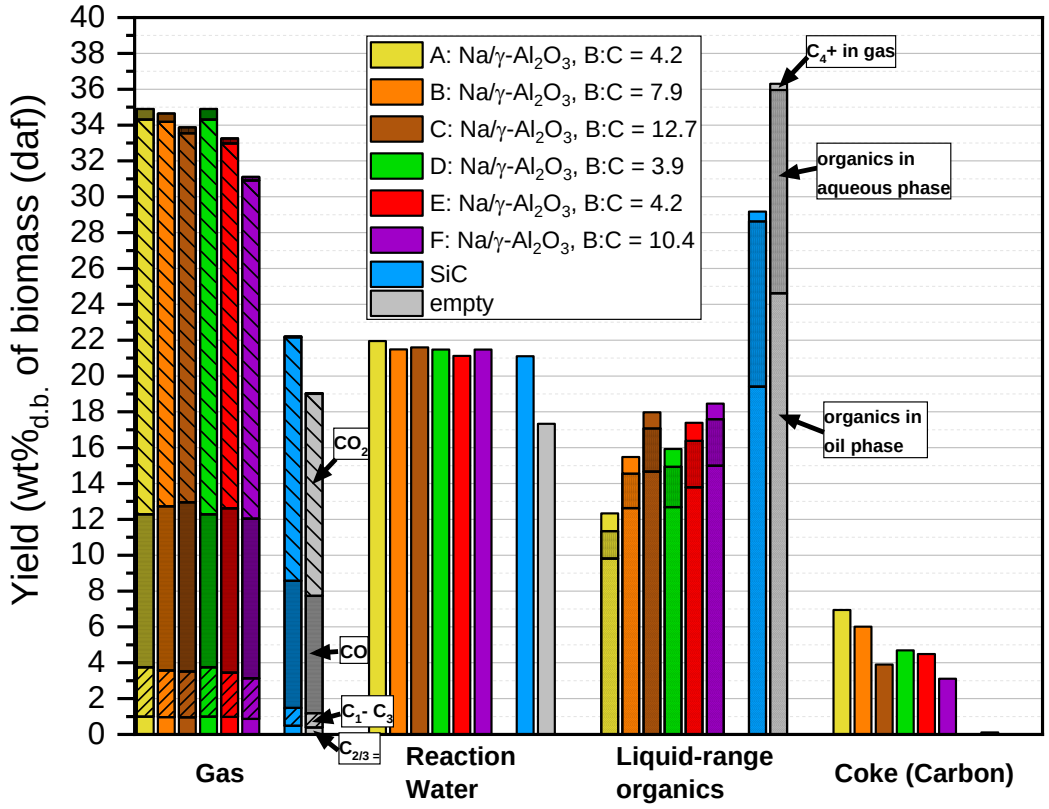

Fig. 3. Product yields based on fed biomass (daf) when passing wheat straw pyrolysis vapors over Na-Al_2O_3. The designation A-F in the legend indicates the order of the performed tests, with the catalyst being regenerated in between each run. Product distribution for SiC (500 °C) and empty catalytic reactor shown for reference. The char yield was 18.7±1.1wt.%.

3.4 Properties of condensed liquid

Table 5 presents an overview of the bio-oil properties along with the B:C ratio at which the oil was obtained and the experiment order . The moisture content of the phase-separated bio-oils was reduced from 11-15 wt.% to 4-9 wt.% after catalytic upgrading. The carbon content of the oils increased from 63 wt.% (empty reactor) to ~78 wt.% upon use of catalyst, while the oxygen content was reduced from 21-27 wt.% to 9-14 wt.%. While no complete deoxygenation was obtained at B:C ~4, the oxygen content remained fairly stable and did not significantly increase with

increasing B:C, as is usually observed with acidic catalysts [18,19,73]. This observation is in line with the ketonization activity observed for the non-condensed vapors analyzed with the μ-Py.

The catalytic treatment increased the HHV from ~30 MJ/kg to ~37 MJ/kg and the effective hydrogen index (EHI) from ~0.6-0.7 to ~1.1-1.2. This is in excellent agreement with the EHI of the non-condensed vapors (**Table 4**). Slightly higher values for the HHV and EHI observed in the bench scale tests could be a result of longer residence times and the exposure of pyrolysis vapors to active sites on the inner surface of tubing in the bench-scale system and the char containing ~25 wt.% ash. In contrast, the μ-Py system is quite inert due to the use of quartz tubes and a shorter char-vapor interaction.

TAN values as low as 0.5 mg KOH/g were obtained, which stresses the selective removal of acids and brings the TAN levels in the same range as acidic crude oil [80]. Also for repeated tests to B:C ~4, the TAN of the oil remained very low, indicating catalyst stability for acid conversion when operated to low B:C. When operated to higher B:C = 10.4 (run F), the TAN had increased to 3.5 mg KOH/g whereas it was 1.3 mg KOH/g for run C (B:C = 12.7). This indicates that the capacity for conversion of acids has decreased slightly after repeated reaction/regeneration cycles, which is likely due to the observed decrease in surface area and basicity (see section 3.1). This is different from what was observed using the μ-Py where the conversion of acids was improved from first to second use. The reason is likely that the catalyst is operated to higher B:C ratio and experiences a higher level of steam for longer time.

The basic nitrogen content on the other hand increased with deoxygenation (from ~0.4 to 0.6 mass%), which indicates that denitrification is more challenging compared to deoxygenation and thus nitrogen compounds were concentrated due to the decrease in oil yield by deoxygenation.

As seen from the weight loss curves during heating of the oils via TGA (see Fig. S12), the volatility and stability of the oils during heating improved significantly. The revaporization efficiency [56,57] stated in **Table 5** indicates how much of the dry organics content in the oil has volatilized at 350 °C. A significant improvement in revaporization efficiency behavior was observed from ~70% to 90-99% upon use of Na-Al_2O_3 catalyst for vapor upgrading, which can be attributed to the reduced charring tendency and reactivity at lower oxygen content.

Table 5. Properties of the phase-separated bio-oil fraction.

Experiment	empty	SiC	A	B	C	D	E	F
B:C		11.0	4.2	7.9	12.7	3.9	4.2	10.4
Yield of oil phase [wt.% (daf)]	24.6	19.4	9.8	12.6	14.6	12.7	13.5	15.0
H_2O [wt.%]	11.0	14.7	4.5	3.9	4.6	3.3	5.9	9.3
wt.% N (d.b.)	3.3	1.6	3.1	3.2	3.5	3.4	2.4	3.5
wt.% C (d.b.)	63.0	69.9	77.8	78.5	78.1	77.5	79.1	78.5
wt.% H (d.b.)	7.2	7.1	9.6	9.3	9.1	9.5	9.0	9.1
wt.% O (d.b.)	26.5	21.4	9.5	9.1	9.2	9.6	9.5	8.9
wt.% S (d.b.)	0.07	0.10	0.35	n.d.	0.15	n.d.	n.d.	n.d.
Higher heating value (HHV) [MJ/kg]	27.7	30.5	37.4	37.4	37.0	37.2	37.1	37.2
EHI	0.59	0.69	1.18	1.14	1.09	1.16	1.16	1.10
TAN [mg KOH/g]	71.1	54.4	0.5	0.7	1.3	1.0	0.9	3.5
Basic nitrogen (mass%)	0.40	0.43	n.d.	0.60	0.66	0.54	0.57	0.61
Revaporization efficiency @350 °C (d.b.)	67	71	99	92	92	99	96	90

The relative abundance of the main compound groups detected by GC-MS/FID in the phase separated aqueous fractions is shown in **Fig. 4**a. A list of the FID areas of the single compounds is found in Table S17, along with the FID response correction taken into account for the effective carbon number of each compound [81]. After upgrading over Na-Al_2O_3, the aqueous phase organics analyzed by GC-FID were mainly comprised of ketones (~55-58%) and alcohols (~34-39%), and smaller fractions of phenols (1-4%) and nitrogen containing compounds (1-3%). Acids such as acetic acid, (methyl-) propanoic acid, butanoic acid, and 2-pyridinecarboxylic acid were

564 only present in small percentages of 2-4% even when operated to high B:C >10. The non-catalytic
565 reference contained significantly more acids (28%). In addition, a high concentration of
566 hydroxyacetone and small amounts of methoxyphenols and anhydro-sugars (especially
567 levoglucosan) were observed, which were not detected in the aqueous fractions derived from Na-
568 Al_2O_3 vapor treatment. Many compounds identified in the aqueous phase of the bench scale tests
569 were also observed in the non-condensed vapors from the μ-Py set up (Fig. S8), such as methanol,
570 ethanol, acetone, hydroxyacetone, acetic and propanoic acid, (methyl)-butanones, pentanones,
571 (methyl)-cyclopentanones, (di-)methyl-2-cyclopenten-1-ones, (methyl)-phenols and methoxy-
572 phenols. **Fig. 4**b shows the semi-quantitative yields by multiplying the yield of total organics (d.b.)
573 in the aqueous phase with the selectivity of identified compounds. Na-Al_2O_3 clearly reduced the
574 yield of acids recovered in the aqueous phase, which also correlates with the low TAN of the phase
575 separated oil phase [19].

576 The selectivity and yields of compounds detected in the oil phase by GC-MS/FID are shown in
577 **Fig. 4**c and d. No acids were detected by GC-MS/FID in the oils obtained with Na-Al_2O_3, even for
578 runs to high B:C. Since some acids were detected in the aqueous phase at B:C ~13 and 10, any
579 small amounts of acids dissolved in the oil-phase may have been below the detection limit of the
580 gas chromatographic method. On the other hand, phenols are known to contribute to the TAN of
581 oils [20] and based on the high selectivity to phenols (**Fig. 4**c) they are likely the main contributors
582 to the remaining TAN of the bio-oils derived from vapor treatment with Na-Al_2O_3.

583 Similar to the considerations made for the μ-Py (section 3.2), the decrease in liquid yield by the
584 catalytic treatment and the increased selectivity to ketones may result in similar overall yields of
585 ketones in the GC-detectable range compared to the non-catalytic case. Therefore, the yield of
586 ketones in the combined liquid phase (oil and aqueous phase) was further divided into ketones

587 with multiple oxygen functionalities and ketones with single oxygen functionalities (see Table
588 S14). At bench scale, no ketones with multiple oxygen functionalities (group i) were detected by
589 GC-MS/FID for the liquid obtained after upgrading with Na-Al_2O_3, while the yield of simple group
590 ii) ketones was equal or higher compared to the non-catalytic reference case (see **Table 6**). Since
591 charring upon heating increases with the oxygen content of oils (see Fig. S11), the presented semi-
592 quantitative yields are likely overestimated for the non-catalytic reference oil/aqueous phase due
593 to their higher charring propensity. Nevertheless, it is clear that the non-catalytic bio-oil contains
594 a cocktail of different oxygenated species and especially higher yields of acids and methoxy-
595 phenols while the Na-Al_2O_3 derived oils mainly contain phenolics and ketones, along with oxygen-
596 free hydrocarbons (between 1.5 and 1.8 wt.% of fed biomass), furans and alcohols.
597 A list of the 24 most prevalent products (constituting ~90% of the total) that were identified in
598 the Na-Al_2O_3 derived bio-oils is provided in Table S18. 17 of these 24 products identified in the
599 condensed oils have also been identified using the μ-Py (Fig. S8, Table S1-S11). Table S19 shows
600 the 20 most prevalent (90% of total) products identified in the bio-oil attained without vapor
601 treatment in the bench scale reactor. 17 of those 20 compounds were also observed for the
602 non-condensed pyrolysis vapors obtained using the μ-Py (Fig. S7, Table S1-S11). Without
603 catalytic treatment, hydroxyacetone and acetic acid appear amongst the highest concentration of
604 compounds for both the non-condensed vapors from the μ-Py and the condensed bio-oil from the
605 bench-Py. As such, there is good agreement in the chemical composition between non-condensed
606 vapors and condensed oils. However, we note that significantly less aldehydes were detected in
607 the condensed non-catalytic pyrolysis oil compared to the non-condensed vapors. Aldehydes are
608 highly reactive and it is therefore likely that aldehydes further reacted/polymerized after
609 condensation.

No methoxy-phenols were detected in the bio-oils from catalytic treatment with Na-Al_2O_3 while methoxy-phenols were found to break through in the non-condensed vapors at B:C >2 using the μ-Py. This observation is attributed to higher conversions obtained in bench scale due to the lower ratio of vapor flowrate to catalyst mass. The removal of the methoxy-groups from methoxy-phenols is in line with higher yields of phenols compared to the non-catalytic reference.

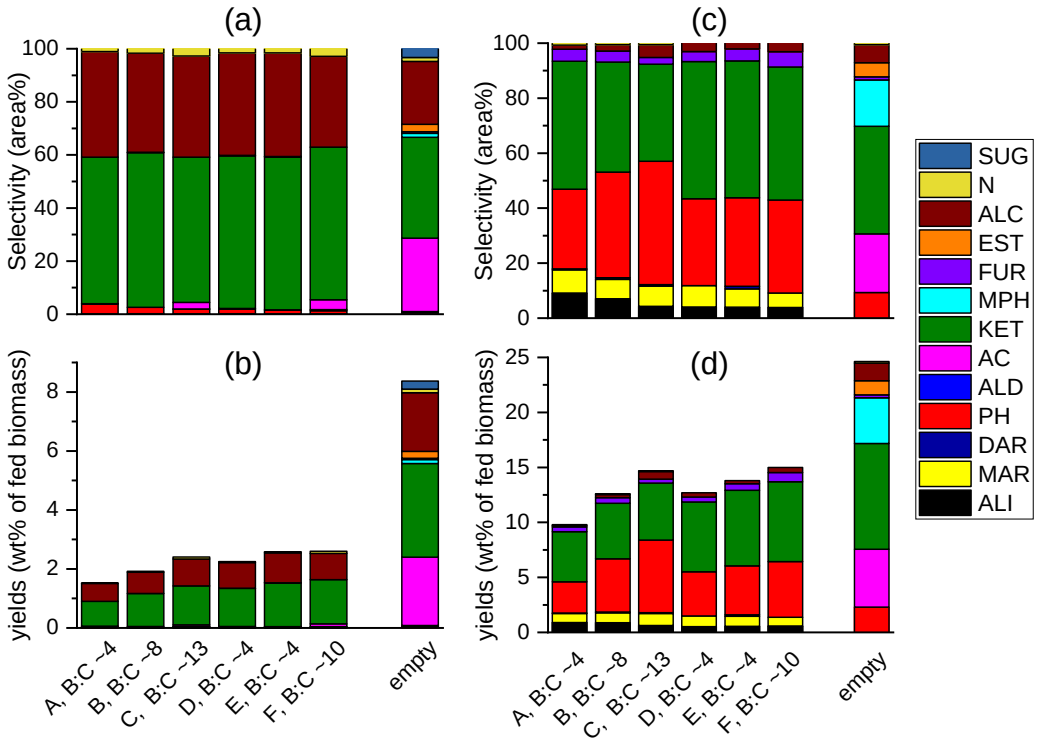

Fig. 4 (a) Selectivity of compounds (grouped) in aqueous phase analyzed by GC-MS/FID. (b) Semi-quantitative yields of compounds in aqueous phase. (c) Selectivity of compounds (grouped) in oil phase analyzed by GC-MS/FID. (d) Semi-quantitative yields of compounds in oil phase.

Table 6. Product yields (wt.% of fed biomass (daf)) of ketones detected in the condensed liquid from bench-Py. Group i) ketones contain multiple oxygen functionalities while group ii) ketones contain only a single ketone group (see Table S14).

	empty reactor	**run A, B:C ~4**	**run B, B:C ~8**	**run C, B:C ~13**	**run D, B:C ~4**	**run E, B:C ~4**	**run F, B:C ~10**
group i) ketones	7.4	0.0	0.0	0.0	0.0	0.0	0.0
group ii) ketones	5.4	5.4	6.2	6.5	7.6	8.4	8.8

623 Two-dimensional GC x GC analysis allows a more comprehensive characterization of bio-oil
624 based on the spatial separation of polar and nonpolar compounds. The 2D GC x GC plots for the
625 non-catalytic bio-oil and the bio-oil obtained from vapor upgrading at run E (B:C ~4) are shown
626 in Fig. S13-S14. The integration results of the different regions in the two-dimensional plots are
627 summarized in **Table 7**. Compared to the non-catalytic reference, the oil obtained from vapor
628 treatment with Na-Al_2O_3 shows increased concentrations of oxygen-free hydrocarbons such as
629 aromatics and paraffins/napthenes. The concentration of carboxylic acids dropped from 5.5% to
630 0.1%, in agreement with the severe reduction in TAN (**Table 5**) and one-dimensional GC-MS/FID
631 (**Fig. 4**) analysis. Likewise, increased contributions of aliphatic ketones (from 3.6 to 14.3%) and a
632 reduction in the concentration of methoxy-phenols (from 10 to 4.4%) agree with the observations
633 made with 1D GC-MS/FID (**Fig. 4**).

634 **Table 7.** Integration results from GC × GC-FID analysis of the bio-oils.

	non-catalytic	run E (B:C ~4)
paraffins/naphthenes	7.1	11.9
alkylbenzenes/naphthenobenzenes	3.9	8.5
diAromatics/triAromatics/Biphenyls	1.4	7.5
carboxylic acids	5.5	0.1
pyrroles/nitriles	1.3	0.6
pentanones/hexanones	14.0	7.1
aliphatic ketone/other aliphatic oxygenates	3.6	14.3
indanones/benzofurans/dibenzofuranes	7.3	11.0
furanones/furfuryl alcohols	2.3	0.1
phenols/methoxybenzenes	29.6	30.9
dihydroxylated benzenes	6.2	0.5
hydroxylated two/three-ring aromatics	7.8	3.1
methoxy-phenols	10.0	4.4

635

636 While gas-chromatographic methods provide single-compound information, they only analyze the
637 more volatile compounds of the oils since compounds may char at the injection port (~280 °C) or
638 have a higher boiling point temperature (Fig. S12). For analysis of the whole oil composition, ^{13}C

NMR characterization was performed for the non-treated bio-oil and two bio-oils obtained by vapor treatment to B:C ~4 and B:C ~10 using 100 g of Na-Al_2O_3 at 500 °C (**Table 8**, Fig. S15). Note that the two oils were obtained towards the end of the test series, i.e. after the catalyst had undergone four or five reaction/regeneration cycles. Despite slight differences in the chemical shift assignment, the ^{13}C NMR analysis of the non-catalytic reference oil agrees well with the ^{13}C NMR analysis reported by Negahdar et al. [63] for wheat straw FP oil, which showed 35.7% alkyl C (54–1 ppm), 12.4% carbonyl (215–163 ppm), 5.6% carbohydrates (103–70 ppm), and 30.1% aromatics (163–103 ppm). The vapor treatment with Na-Al_2O_3 reduced the contribution of carbonyls from ~15% to ~11% and the contribution of aromatic C–O was reduced from ~13 to 7-8%. Nguyen et al. [46] reported that the upgraded oil from treatment of pine FP vapors with 20 wt.% Na_2CO_3/γ-Al_2O_3 catalyst contained a high amount of carbonyl components in the bio-oil, which can cause stability problems owing to condensation reactions with alcohols/phenols. The present ^{13}C NMR analysis shows that for upgrading of wheat straw derived FP vapors using the Na-Al_2O_3 catalyst the concentration of carbonyl and phenols was reduced by the catalytic treatment, implying improved stability. However, carbonyls were not very effectively removed with Na-Al_2O_3, which is in agreement with a high yield of ketones observed with the μ-Py (**Fig. 2**, **Table 3**) and the GC analysis of the condensed aqueous and oil phase (**Fig. 4**). The almost complete removal of acids and increased CO_2 yields suggests ketonization, and the ketones were not efficiently deoxygenated further over the Na-Al_2O_3 catalyst. It is worth mentioning that the increase in aliphatics detected by NMR could indicate the presence of long aliphatic chains (with or without oxygen functionality) and more methyl-groups, which in combination with the increased concentration of aliphatic ketones detected by GC x GC analysis agrees with the

increased concentration of methylated cyclopentenones and long chain aliphatic ketones observed with the μ-Py.

The sum of aromatic C-C and C-H contributions increased by the catalytic treatment from ~25% for the non-catalytic case to ~28–29% (in agreement with higher yields of MAR and PH observed by GC-MS/FID, **Table 5**), along with a clear increase in the aliphatic C–H contribution from ~32% to ~50%. The catalytic treatment reduced the aliphatic C–O contribution from ~11 to ~2% and methoxy groups were practically removed completely. While a slight increase in aromatic C–O and methoxy groups is observed when comparing the oils obtained at B:C ~4 and B:C ~10, the oils are surprisingly similar, which indicates that the Na-Al_2O_3 catalyst can maintain its catalytic performance up to high B:C ratios.

Table 8. Carbon percentage based on the ^{13}C NMR analysis of bio-oils.

	-	Na-Al_2O_3, B:C ~4	Na-Al_2O_3, B:C ~10
Carbonyl (215–166.5 ppm)	14.6%	11.2%	10.7%
Aromatic C–O (166.5–142 ppm)	12.5%	6.9%	8.2%
Aromatic C–C (142–132/125 ppm)[a]	7.5%	4.8%	5.1%
Aromatic C–H (132/125–95.8 ppm)[a]	17.9%	23.0%	24.3%
Aliphatic C–O (95.8–60.8 ppm)	10.6%	2.2%	2.2%
Methoxy (60.8–55.2)	5.0%	0.4%	0.6%
Aliphatic C–H (55.2–0 ppm, with exclusion of solvent)	31.8%	51.4%	48.8%

[a]For catalytically treated pyrolysis oils, the border between aromatic C–C and aromatic C–H was moved downfield from 125 ppm to 132 ppm following the recommendation of Happs et al. [59]

Compared to 1D NMR spectra required for quantification, 2D NMR spectra lower the likelihood of overlapping because the signals are spread out into two dimensions. The heteronuclear single-quantum correlation spectroscopy (HSQC) correlates chemical shifts of carbons and protons in a phase sensitive way. The 2D HSQC spectra are provided in Fig. S16. Oils obtained from the catalytic vapor treatment with Na-Al_2O_3 showed a clear reduction in -CH-O- and -O-CH-O- groups, mainly present in sugars. In addition, a clear reduction in aldehydes is observed. For the

oil collected at B:C ~10, a slightly higher contribution of -CH-O-, -O-CH-O-, and aldehyde groups is noted compared to B:C ~4; however the concentration of these groups at B:C ~10 was still clearly lower compared to the non-catalytic reference.

3.5 Coke on catalyst

The combustion of the coke deposits that had accumulated on 2 mg of catalyst (tested at the μ-Py) was monitored by thermogravimetric analysis (**Fig. 5**). Coke deposits on Na-Al_2O_3 (5.9 wt.% of C per coke-free catalyst) combusted at ~100 °C lower temperature compared to γ-Al_2O_3 (8.0 wt.% of C per coke-free catalyst), which can be attributed to a combustion catalytic effect of Na [82]. In combination with the lower coke yields observed after Na incorporation (**Table 4**), this demonstrates that the Na incorporation could decrease regeneration time.

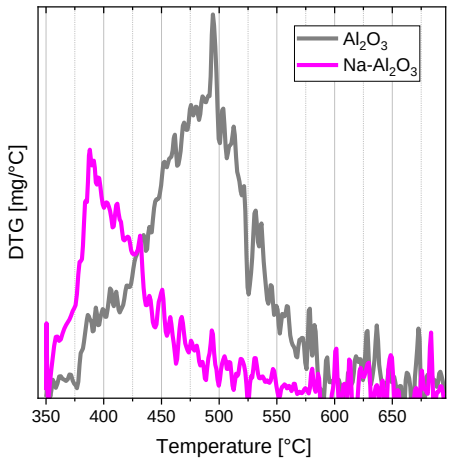

Fig. 5. Derivative curves of weight loss (DTG) during combustion of coke deposits on 2 mg of catalyst. The coke deposited on the catalyst during upgrading of wheat straw FP vapors (B:C ~4) in a μ-Py. Reaction atmosphere during coke combustion: 20 vol.% O_2 in argon, heating rate: 10 °C/min.

Fig. 6 compares the coking propensity (in terms of deposited mass of carbon per coke-free catalyst) for different catalysts from the bench scale pyrolyzer as a function of increasing B:C ratios. When using Na-Al_2O_3 for vapor treatment, the first test at B:C ~4 (run A) formed more coke compared to later repetitions at B:C ~4 (run D+E), which is tentatively attributed to the observed decrease in the amount of basic sites and surface area. Our earlier works [18,19,73]

699 indicated that increased catalyst loadings resulted in increased amounts of coke deposited per mass
700 of catalyst (compared at the same B:C). In earlier work [19] the coke deposition on γ-Al_2O_3 was
701 determined for ~180 and ~40 g, while in this work 100 g of Na-Al_2O_3 was tested. As seen from
702 **Fig. 6**, the coking propensity of Na-Al_2O_3 appears in the same range as for alumina and about
703 twice as high compared to HZSM-5 zeolite. While for the initial tests (A+B) the coking propensity
704 for 100 g Na-Al_2O_3 was higher compared to using ~180 g γ-Al_2O_3, later tests (D-F) indicate a
705 coking propensity similar to ~40 g γ-Al_2O_3, which suggests that for the same mass of catalyst the
706 'equilibrated' Na-Al_2O_3 has a slightly lower coking propensity compared to γ-Al_2O_3. It is well
707 known that sodium and potassium are very reactive towards steam gasification of char [83]. Under
708 reaction conditions, the moisture introduced by the biomass (~9 wt.%) and the water produced
709 from dehydration reactions occurring during catalytic vapor upgrading contribute to a high steam
710 partial pressure (~14%). While gasification usually operates at >800 °C, we tested to what extent
711 coke gasification catalyzed by Na occurs at the reaction temperature of ~500-530 °C applied in
712 this work. To this end, steam (~36 vol.%) was passed over a coked Na-Al_2O_3 catalysts with ~32
713 wt.% coke/catalyst that was recovered after test F (B:C ~10) while increasing the catalyst
714 temperature from 120 °C to 550 °C at 2 °C/min. Monitoring the gas species during the temperature
715 ramp (Fig. S17) confirmed that towards the reaction temperature applied for the vapor upgrading,
716 appreciable coke gasification reactions take place over the Na-Al_2O_3 catalyst. Besides CO_2, also
717 CO, small hydrocarbons (mainly methane), and H_2 were observed, especially towards increased
718 temperature. H_2 may be the product from gasification and/or WGS. While the steam concentration
719 was ~14% under reaction conditions in this study, at full scale less nitrogen carrier gas and thus
720 higher steam loadings are expected.

For the coked catalyst collected after run F (B:C = 10.4), the surface area had decreased from ~100 m^2/g (coke-free catalyst) to 53 m^2/g (coked catalyst), and the pore volume had decreased from ~0.28 to 0.11 cc/g, indicating that the coke had filled ~0.17 cc/g of the pores. While the pore volume decreased, there was no significant shift in the pore width centered at ~105 Å (see Fig. S3). Nguyen et al. [46] found that the coke species contained a high oxygen content of ~42 wt.% due to the oligomerization of pyrolysis vapor oxygenates. In contrast to their findings, our results showed that the coke deposited on Na-Al_2O_3 from upgrading of wheat straw FP vapors at bench scale contained 94 wt.% C, 2 wt.% H, and only ~4 wt.% oxygen (by difference). In agreement with the lower combustion temperature for regeneration of Na-Al_2O_3 compared to γ-Al_2O_3 used at the μ-Py (**Fig. 5**), the evolution of CO/CO_2 during regeneration of Na-Al_2O_3 used at bench scale occurred at lower temperatures compared to the regeneration of Al_2O_3 (see Fig. S18).

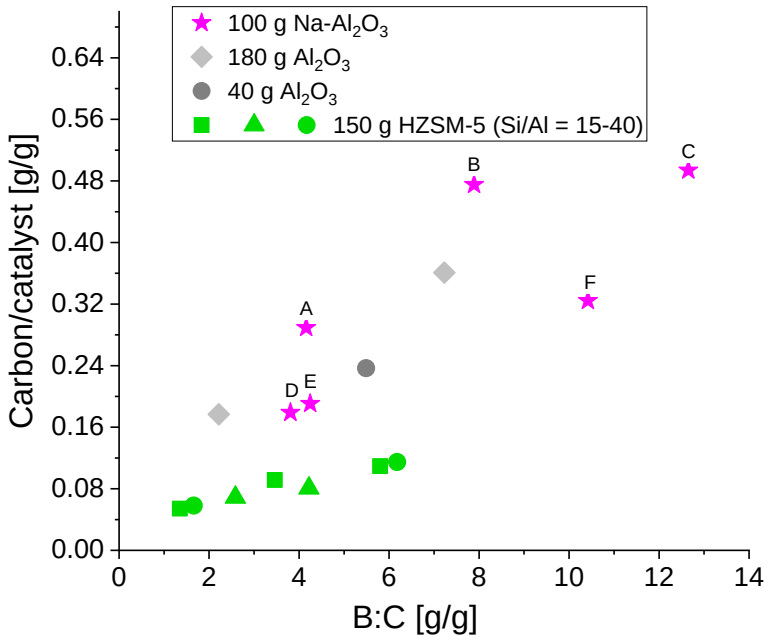

Fig. 6. Deposited mass of carbon in coke per coke-free catalyst for different catalysts and increasing B:C ratios for the bench scale pyrolyzer set-up. The letter next to the data points obtained with Na-Al_2O_3 indicates the order in which the experiments were performed. Data points for γ-Al_2O_3 and HZSM-5 have been reported in earlier works [19,73].

3.6 Catalyst stability

SEM-EDX analysis showed that for the fresh catalyst the Na is homogenously distributed (**Fig. 7**a) on the γ-Al_2O_3 support, in agreement with literature [46]. Please note that the color intensity in **Fig. 7** is not representative of the quantitative elemental composition of the sample. Further SEM-EDX examples showing the distribution of Al, O, and Na are provided in Fig. S19.

The catalyst underwent six cycles of reaction and regeneration, with a nominal set-point of 500 and 550 °C, respectively. Due to exothermic reactions during vapor upgrading and coke combustion, the catalyst experienced a maximum temperature of ~530 °C and ~570 °C during the reaction and regeneration, respectively. The biomass introduced moisture and the pyrolysis reactions produce steam during FP operation, while during regeneration steam is produced via combustion of hydrogen in the coke. It can be seen from **Fig. 7**b and Fig. S19 that also after the exposure to hydrothermal conditions during reaction/regeneration the Na was homogeneously dispersed on the γ-Al_2O_3 support at micron length scale. The surface area of Na-Al_2O_3 slightly decreased after six reaction/regeneration cycles from 125 m^2/g to 100 m^2/g, which may indicate sintering of the alumina.

In order to ensure that no Na species were lost due to volatilization during reaction and regeneration, the Na content was re-analyzed after the test series. In addition, the used catalyst was analyzed for components that are present in high concentrations in the biomass ash (Ca, K, and Mg). As shown in **Table 9**, no reduction in Na content has occurred—in agreement with others [45]— and any accumulation of biomass ash components was successfully prevented by the ex-situ configuration of the catalyst bed with an upstream hot gas filtration at 350 °C.

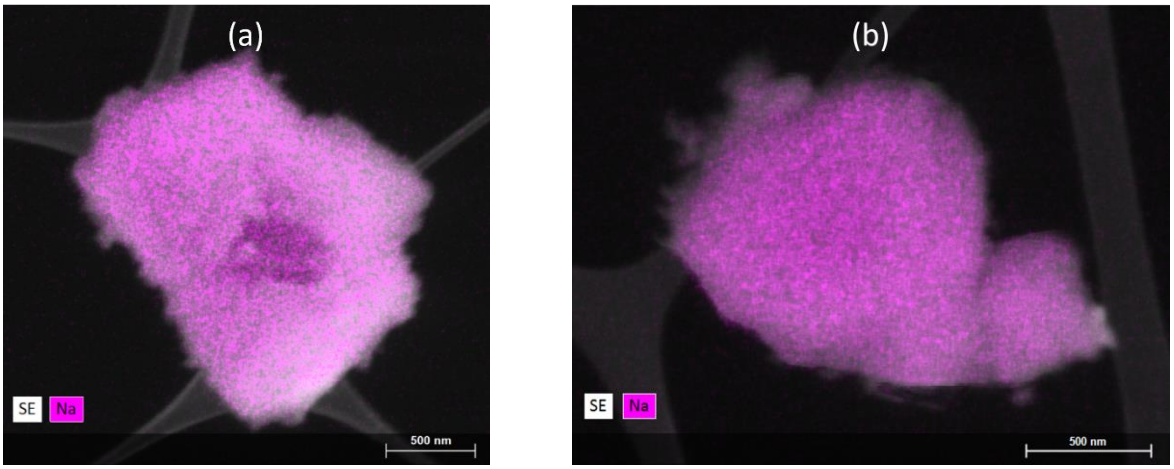

Fig. 7. SEM-EDX images of Na-Al_2O_3 catalyst (a) pre-reaction and (b) post-reaction. The color intensity is not representative for the quantitative elemental composition of the sample.

Table 9. Elemental analysis by XRF of Na-Al_2O_3 catalyst before and after test series.

	Al (wt.%)	Si (wt.%)	Na (wt.%)	Ca (wt.%)	K (wt.%)	Mg (wt.%)
Na-Al_2O_3	43.6	n.d.	9.55	n.d.	n.d.	n.d.
Na-Al_2O_3-6u-6r[†]	41.3	0.1	10.6	<0.05	<0.04	0.00

[†]The suffix '6u-6r' indicates that the catalyst was used for six cycles of vapor upgrading and regeneration.

For the basicity probed by CO_2-TPD, the adsorption of CO_2 was conducted at 50 °C. In order to investigate any differences in the CO_2 chemisorption capability under operating conditions (500 °C) after six reaction-regeneration cycles, the evolving CO_2 during heating to 600 °C was monitored. The results of this investigation are shown in Fig. S20. Two distinct CO_2 desorption peaks at ~250 °C and ~330 °C were observed for the calcined Na-Al_2O_3, which had been exposed to air, in agreement with weight losses at similar temperatures observed with the TGA (Fig. S5). After lowering the sample temperature to 500 °C, adsorption of CO_2 (in 100 % CO_2) and flushing of weakly adsorbed CO_2 in helium, the further increase in temperature showed a clear release of CO_2 at ~590 °C (see Fig. S20). This sequence was repeated twice for the same Na-Al_2O_3 catalyst after being exposed to ambient air over night, by which CO2 was re-adsorbed. As seen from Fig. S20, the calcined Na-Al_2O_3 catalyst gradually lost its capacity for CO_2 adsorption from ambient

774 air, whereas the CO_2 adsorption capacity at 500 °C remained at a similar level. Similarly, for the
775 sample obtained after six reaction-regeneration cycles, there was less CO_2 desorption during the
776 initial heating ramp, while the catalyst still showed a good uptake of CO_2 at 500 °C. For Al_2O_3 on
777 the other hand, the adsorption of CO_2 from ambient air and under reaction conditions was
778 significantly less (Fig. S20).

779 The concentration of CO_2 measured during the in situ XRD tests with the calcined Na-Al_2O_3 and
780 Na-Al_2O_3-u6-r6 is shown in Fig. S21. In agreement with Fig. S20, the fresh sample and Na-Al_2O_3-
781 u6-r6 have a similar capacity for CO_2 adsorption at 500 °C, indicating that this feature of the
782 catalyst is stable under the applied reaction and regeneration conditions.

783 The XRD patterns obtained during the situ XRD test are shown in Fig. S22 and S23, and a
784 selection of the in situ XRD patterns are shown in **Fig. 8** and **Fig. 9**. For both samples, there was
785 no drastic shift in peak positions over the course of the experiment, but no single phase was found
786 that would fit all the additional Bragg reflections. The prominent peaks observed at ~15.6° and
787 ~32.2° for the XRD pattern that was acquired in ambient air using the pressed pellet (Fig. S6) were
788 absent when the same sample was analyzed in powder form using the in situ XRD apparatus. This
789 difference is tentatively attributed to differences in ambient humidity and thus the extent of
790 hydration of Na-related species on the sample, e.g. the prominent peaks observed at ~15.6° and
791 ~32.2° may correspond to NaOH and hydrated Na_2CO_3, respectively.

792 After CO_2 adsorption at 500 °C using the in situ XRD, two new peaks, likely related to Na_2CO_3,
793 appeared at 27.2° and 33.7° for the calcined sample, which then disappeared again once heated
794 further to 600 °C in He. For the Na-Al_2O_3-u6-r6 sample, this feature could not be discerned, even
795 though at 500 °C it had adsorbed a similar level of CO_2 (see Fig. S21). This could indicate a
796 decrease in crystallite-size of the Na_2CO_3-related phase after six reaction-regeneration cycles or

the binding of CO_2 to a different phase. At high temperature of 600 °C and He flow, the intensity of the peak at ~26.7° increased for the fresh sample, while this effect was less pronounced for Na-Al_2O_3-u6-r6. Furthermore, the intensity of peaks at 20.4° and 29.8° was much higher for sample Na-Al_2O_3-u6-r6 compared to the calcined sample, and Na-Al_2O_3-u6-r6 showed a much higher intensity of the three peaks in the region 33–35° (see **Fig. 9**), indicating that differences in the distribution between different phases have occurred during the six reaction-regeneration cycles.

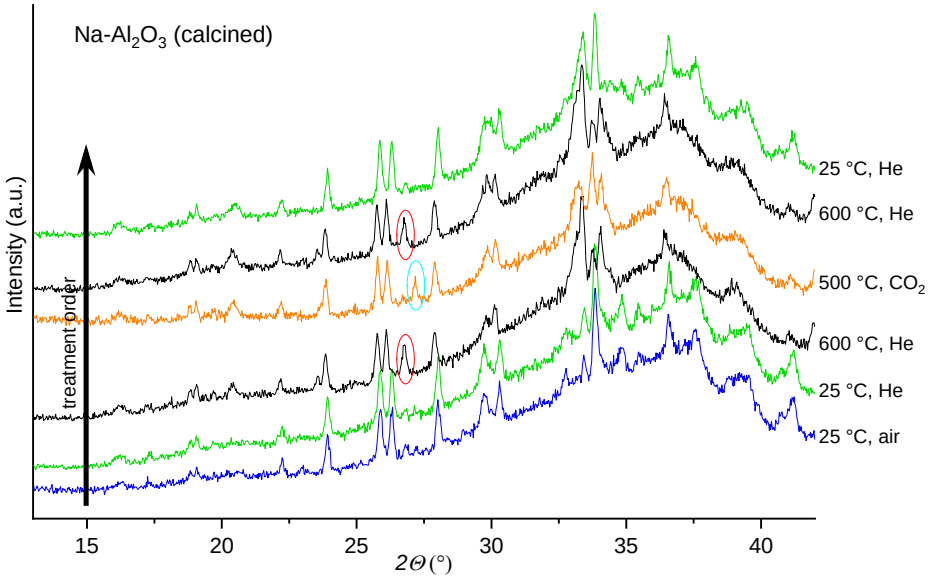

Fig. 8. XRD patterns acquired at the indicated temperature and reaction atmosphere for the calcined Na-Al_2O_3 catalyst. The peak appearing at high temperature of 600 °C under He atmosphere is marked in a red ring, and the peak appearing with CO_2 adsorption at 500 °C is marked in a blue ring.

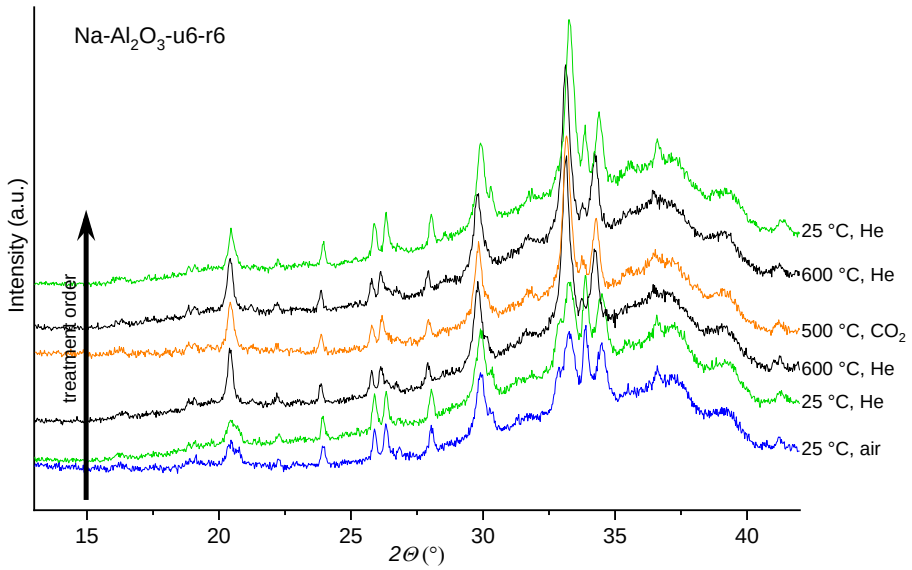

Fig. 9. XRD patterns acquired at the indicated temperature and reaction atmosphere for Na-Al_2O_3 catalyst after six reaction-regeneration cycles.

3.7 Performance of Na-Al_2O_3 in comparison with acidic catalysts

Fig. 10a shows the degree of vapor deoxygenation (DOD) and the relative energy recovery of the vapors compared to a non-catalytic reference case for the μ-Py study. For γ-Al_2O_3, ~30% DOD was obtained for the first vapor pulse at ~50% energy recovery of the vapors. With increasing B:C, the DOD continuously decreased while the energy recovery of the vapors increased. For Na-Al_2O_3, on the other hand, the initial DOD was lower at ~22%. Importantly however, it remained stable for increasing B:C.

It is of interest to compare the performance of the Na-Al_2O_3 tested in the bench-Py to other acidic catalysts. In earlier work [19,73], we reported the performance of HZSM-5, γ-Al_2O_3, mesoporous HZSM-5, and HZSM-5/γ-Al_2O_3 for upgrading of wheat straw FP vapors. In comparison with these catalysts, **Fig. 10**b shows the degree of deoxygenation (DOD) obtained in the collected bio-oil and their energy recovery with respect to a non-catalytic reference case (empty catalytic reactor at 500 °C). For acidic catalysts, with operation to increasing B:C the energy recovery of the oil increased while the DOD clearly decreased. For Na-Al_2O_3, however, the DOD remained stable between 60

824 to 70%, even when operated to quite high B:C of ~13. This allowed outperforming the acidic
825 catalysts, since about 10% higher energy recovery was obtained for the same DOD of ~60%.
826 While overall higher deoxygenation was obtained at bench-Py due to the higher ratio of catalyst
827 mass to vapor flowrate, we find that the μ-Py can provide reasonable indications for the trends in
828 deoxygenation performance of different catalysts. When Na-Al_2O_3 was tested at the bench-Py, it
829 is interesting to note that the oil yield (see **Table 5**) and thus the energy recovery increased for the
830 same B:C of 4 after repeated use. This observation correlated with decreased yields of coke and
831 gas after repeated use (see **Fig. 3**). Nguyen et al. [51] found the deoxygenation activity of the 25
832 wt.%Na_2CO_3/γ-Al_2O_3 catalyst comparable to HZSM-5 (Si/Al ~ 15), albeit the Na-Al_2O_3 catalyst
833 showed a higher coke yield (4.1 wt.%) compared to HZSM-5 (2.3 wt.%) and a lower yield of
834 organic fraction (26.2 wt.% vs. 27.8 wt.%).
835 **Fig. 11** shows the obtained TAN of the collected bio-oils from upgrading with Na-Al_2O_3 and
836 solid acid catalysts [19,73] with the cumulative B:C ratio to which the process was operated and
837 the corresponding yield of oil fraction. As seen from **Fig. 11**a, in comparison to the reference acidic
838 catalysts the bio-oil obtained from vapor treatment with Na-Al_2O_3 has a lower TAN for the whole
839 range of B:C 4–13. Importantly, for a given TAN of the bio-oil, higher oil yields were obtained
840 with Na-Al_2O_3 compared to using acidic catalysts (**Fig. 11**b).

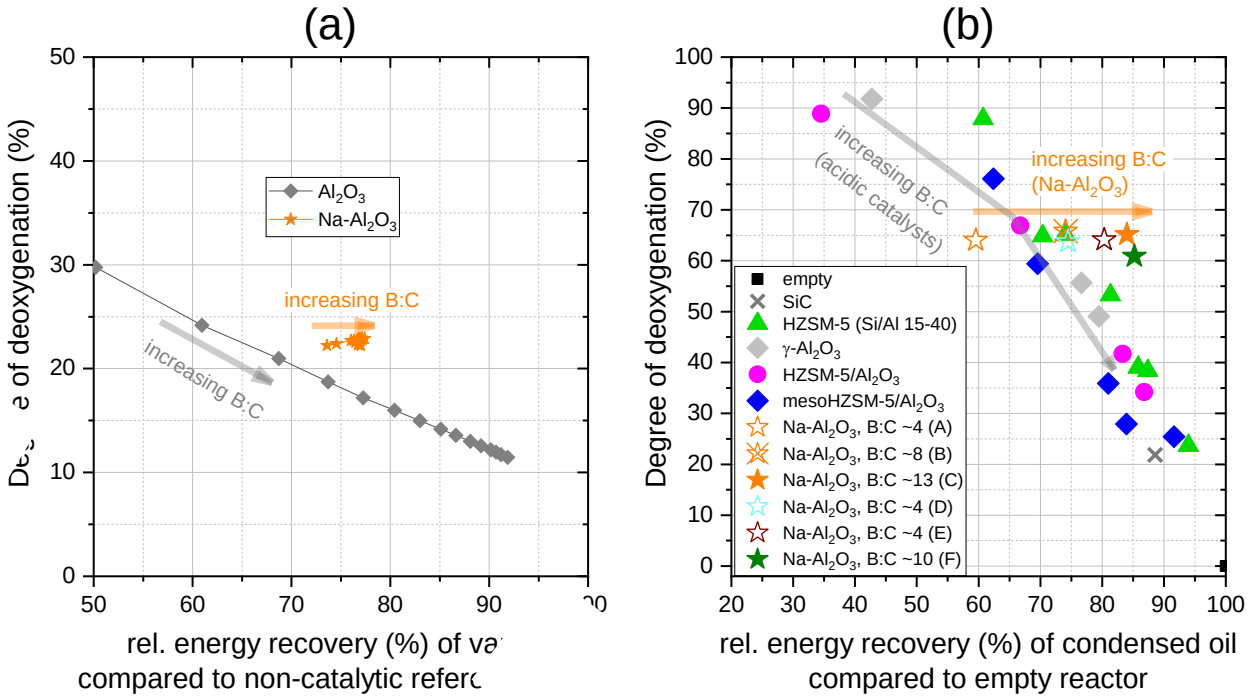

841

842 **Fig. 10**. Relative deoxygenation and energy recovery of (a) non-condensed vapors in µ-Py and (b) of the
843 condensed oil phase including C_4+ gas compounds compared to a non-catalytic reference in bench scale.
844 Note the difference axes scaling in **Fig. 10**a and b. Data points for acidic catalysts shown in **Fig. 10**b have
845 been reported in earlier works [19,73]. For brevity, the results obtained with different HZSM-5 with Si/Al
846 of 15, 27, and 40 are represented in one symbol.

847

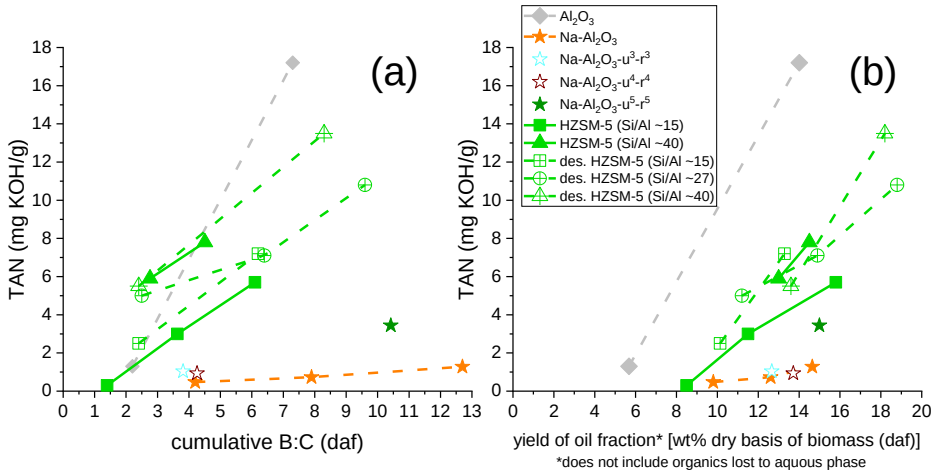

848

849 **Fig. 11. (a)** Total acid number (TAN) of collected oils as a function of cumulative biomass-to-catalyst ratio.
850 **(b)** TAN as a function of oil yield. The yield and TAN of the bio-oil without vapor treatment was 25 wt.%
851 and 71 mg KOH/g, respectively.

4 CONCLUSIONS

The upgrading of pyrolysis oil by using Na-doped γ-Al_2O_3 as a catalyst for deoxygenation of wheat straw fast pyrolysis vapors was investigated by analytical pyrolysis (μ-Py) and a larger bench scale pyrolysis unit. Na impregnation of mesoporous γ-Al_2O_3 influenced the textural and chemical properties; in particular, the surface area and acidity decreased, while basicity was added. The Na species were well distributed over the support. By using the μ-Py, the effect of catalyst deactivation on the change in product composition was monitored for the non-condensed vapors. Acids were effectively converted up to higher biomass-to-catalyst ratios for Na-Al_2O_3 compared to γ-Al_2O_3. The high yield of ketones and CO_2 strongly suggested ketonization-activity, which was confirmed by feeding carboxylic acid model compounds. No permanent catalyst deactivation was observed after a single regeneration. The yield of coke was lower than for γ-Al_2O_3, possibly due to Na-catalyzed gasification by steam during operation, and regeneration by combustion was shifted to lower temperatures, similarly catalyzed by Na.

Bench scale tests using 100 g of catalysts allowed assessing the fuel properties and energy recovery of condensed pyrolysis oil, which are relevant parameters for industrial applications. When operated to a biomass to catalyst ratio (B:C) of ~4 g/g, the bio-oil had remarkably low TAN of ~1 mg KOH/g and a 65% lower oxygen content compared to a non-catalytic oil. The catalyst activity for acid conversion was stable for multiple reaction/regenerations cycles and the Na remained well dispersed on the support despite the hydrothermal conditions of ~530 °C during reaction and ~570 °C during regeneration. However, compared to the freshly calcined catalyst, a decrease in basicity and an increase in acidity was observed indicating that (part of) the Na was bound differently after repeated use.

874 Compared to acidic catalysts such as γ-Al_2O_3 or HZSM-5 zeolite, the oxygen removal with Na-
875 Al_2O_3 was less severe at low B:C, limited to producing a bio-oil with ~9 wt.% O at the applied
876 flow to catalyst ratio. This is attributed to the ketonization activity of Na-Al_2O_3, retaining oxygen
877 in the formed ketones. However, at energy recoveries of ~60-70% relative to non-treated bio-oil,
878 the deoxygenation was comparable to the acidic catalysts. The operation to higher B:C ratios up
879 to 13 maintained a good deoxygenation performance of ~60%, which allowed to achieve ~10%
880 higher energy recovery of bio-oil compared to the acidic catalysts. For a given TAN, the use of
881 Na-Al_2O_3 allowed to operate to higher B:C ratios and provided higher oil yield compared to vapor
882 treatment with acidic catalysts. As such, the upgrading of biomass derived fast pyrolysis vapors
883 with Na-Al_2O_3 poses an economically attractive alternative to zeolites for production of bio-oil
884 with low corrosion potential, which may be further processed in conventional refineries or directly
885 applied as a renewable fuel for ship diesel engines. Further studies of Na-Al_2O_3 to elucidate its
886 structure, optimal Na content, long-term behavior and processing of the bio-oil in refinery
887 processes such as FCC and hydroprocessing appear highly relevant.

ASSOCIATED CONTENT

Supporting Information

Micro-pyrolyzer scheme; list of compounds detected in non-condensed vapors; product uncertainty of μ-Py; scheme of bench-scale fast pyrolysis unit; Isotherms and pore size distribution from N_2 physisorption; NH_3-TPD of catalysts used in μ-Py; thermo-gravimetric analysis of catalysts; GC-FID chromatograms obtained in μ-Py; change in carbon yield and acid concentration of vapors; Catalyst temperature and gas concentration during continuous vapor treatment at bench scale; thermo-gravimetric analysis of bio-oils; ; list of compounds detected in condensed aqueous and oil phase; ^{13}C NMR and 2D NMR spectra of bio-oils; CO and CO_2 evolution during coke combustion; SEM-EDX images of fresh and used catalysts;

AUTHOR INFORMATION

Corresponding Author:

* aj@kt.dtu.dk (Anker Degn Jensen)

Author Contributions

The manuscript was written through contributions of all authors. All authors have given approval to the final version of the manuscript.

Funding Sources

Andreas Eschenbacher acknowledges funding by the Danish Energy Technology Development and Demonstration Program (EUDP project number 12454). Alireza Saraeian and Brent H. Shanks would like to acknowledge funding from the Iowa Energy Center, Iowa Economic Development Authority and its utility partners under the grant number 17-IEC-002.

ACKNOWLEDGMENT

The help of Dr. Leonhard Schill (DTU, Department of Chemistry) with conducting the CO_2-TPD measurements is gratefully acknowledged.

ABBREVIATIONS

AC, acids; ALC, alcohols; ALD, aldehydes; ALI, aliphatics; BTX, benzene, toluene and xylenes; CFP, catalytic fast pyrolysis; daf, dry and ash-free; DAR, diaromatics; d.b., dry basis; DTG, derivative thermogravimetry; EST, esters; FID, flame ionization detection; FUR, furans; GC, gas chromatography; KET, ketones; MAR, monoaromatics; MPH; methoxy-phenolics; MS, mass spectrometry; N, nitrogen containing compound; n.d., not determined; μ-Py, micro-pyrolyzer, PH, phenolics; SUG, sugars; TEM, transmission electron microscopy; TGA, thermogravimetric analysis; TPD, temperature-programmed desorption;

REFERENCES

[1] G.W. Huber, A. Corma, Synergies between bio- and oil refineries for the production of fuels from biomass, Angew. Chemie - Int. Ed. 46 (2007) 7184–7201. doi:10.1002/anie.200604504.

[2] N. Tröger, D. Richter, R. Stahl, Effect of feedstock composition on product yields and energy recovery rates of fast pyrolysis products from different straw types, J. Anal. Appl. Pyrolysis. 100 (2013) 158–165. doi:10.1016/j.jaap.2012.12.012.

[3] C.W. Edmunds, E.A.R. Molina, N. Andre, C. Hamilton, S. Park, O. Fasina, S. Adhikari, S.S. Kelley, J.S. Tumuluru, T.G. Rials, N. Labbe, Blended Feedstocks for Thermochemical Conversion: Biomass Characterization and Bio-Oil Production From Switchgrass-Pine Residues Blends, Front. Energy Res. 6 (2018) 16. doi:10.3389/fenrg.2018.00079.

[4] K. Wang, O.D. Mante, J.E. Peters, D.C. Dayton, Influence of the Feedstock on Catalytic Fast Pyrolysis with a Solid Acid Catalyst, Energy Technol. (2016) 183–188. doi:10.1002/ente.201600254.

[5] D.L. Carpenter, T.L. Westover, S. Czernik, W. Jablonski, Biomass feedstocks for renewable fuel production: a review of the impacts of feedstock and pretreatment on the yield and product distribution of fast pyrolysis bio-oils and vapors, Green Chem. 16 (2014) 384–406. doi:10.1039/C3GC41631C.

[6] B. Rejai, S.C.S.C.S.C. Engineer, R.J. Evans, S. Chemist, P. Chemist, J.P. Diebold, P.C. Engineer, J.W. Scahill, S.C.S.C.S.C. Engineer, C. Conversion, The conversion of biobased feedstocks to liquid fuels through pyrolysis, Energy From Biomass Wastes XV. (1991) 855–876.

[7] T.N. Trinh, P.A. Jensen, D.J. Kim, N.O. Knudsen, H.R. Sørensen, S. Hvilsted, Comparison of lignin, macroalgae, wood, and straw fast pyrolysis, Energy and Fuels. 27 (2013) 1399–1409. doi:10.1021/ef301927y.

[8] C.E. Greenhalf, D.J. Nowakowski, A.B. Harms, J.O. Titiloye, A. V. Bridgwater, A comparative study of straw, perennial grasses and hardwoods in terms of fast pyrolysis products, Fuel. 108 (2013) 216–230. doi:10.1016/j.fuel.2013.01.075.

[9] H.L. Chum, R.P. Overend, Biomass and renewable fuels, Fuel Process. Technol. 71 (2001) 187–195. doi:10.1016/S0378-3820(01)00146-1.

[10] M. Shemfe, S. Gu, B. Fidalgo, Techno-economic analysis of biofuel production via bio-oil zeolite upgrading: An evaluation of two catalyst regeneration systems, Biomass and Bioenergy. 98 (2017) 182–193. doi:10.1016/j.biombioe.2017.01.020.

[11] L. Faba, E. Díaz, S. Ordóñez, Recent developments on the catalytic technologies for the transformation of biomass into biofuels: A patent survey, Renew. Sustain. Energy Rev. 51 (2015) 273–287. doi:10.1016/j.rser.2015.06.020.

[12] M.S. Talmadge, R.M. Baldwin, M.J. Biddy, R.L. McCormick, G.T. Beckham, G.A. Ferguson, S. Czernik, K. Magrini, T.D. Foust, P.D. Metelski, C. Hetrick, M.R. Nimlos, A perspective on oxygenated species in the refinery integration of pyrolysis oil, Green Chem. 16 (2014) 407–453. doi:10.1039/C3GC41951G.

[13] M.P. Brady, J.R. Keiser, D.N. Leonard, A.H. Zacher, K.J. Bryden, G.D. Weatherbee, Corrosion of stainless steels in the riser during co-processing of bio-oils in a fluid catalytic cracking pilot plant, Fuel Process. Technol. 159 (2017) 187–199. doi:10.1016/j.fuproc.2017.01.041.

[14] A. Pinho, M.B.B. de Almeida, F.L. Mendes, L.C. Casavechia, M.S. Talmadge, C.M. Kinchin, H.L. Chum, A. De Rezende, M.B.B. De Almeida, F. Leal, L. Carlos, M.S. Talmadge, C.M. Kinchin, H.L. Chum, Fast pyrolysis oil from pinewood chips co-processing with vacuum gas oil in an FCC unit for second generation fuel production, Fuel. 188 (2017) 462–473. doi:10.1016/j.fuel.2016.10.032.

[15] T. Marker, J. Petri, T. Kalnes, M. McCall, D. Mackowiak, B. Jerosky, B. Reagan, L. Nemeth, M. Krawczyk, S. Czernik, D.C. Elliott, D. Shonnard, Opportunities for Biorenewables in Oil Refineries, Golden, CO, 2005. doi:10.2172/861458.

[16] A. V. Bridgwater, Review of fast pyrolysis of biomass and product upgrading, Biomass and Bioenergy. 38 (2012) 68–94. doi:10.1016/j.biombioe.2011.01.048.

[17] R. French, S. Czernik, Catalytic pyrolysis of biomass for biofuels production, Fuel Process. Technol. 91 (2010) 25–32. doi:10.1016/j.fuproc.2009.08.011.

[18] A. Eschenbacher, P.A. Jensen, U.B. Henriksen, J. Ahrenfeldt, C. Li, J.Ø. Duus, U.V. Mentzel, A.D. Jensen, Impact of ZSM-5 deactivation on bio-oil quality during upgrading of straw derived pyrolysis vapors, Energy & Fuels. 33 (2019) 397–412. doi:10.1021/acs.energyfuels.8b03691.

[19] A. Eschenbacher, P.A. Jensen, U.B. Henriksen, J. Ahrenfeldt, C. Li, J.Ø. Duus, U.V. Mentzel, A.D. Jensen, Deoxygenation of wheat straw fast pyrolysis vapors using HZSM-5, Al2O3 , HZSM-5/Al2O3 extrudates, and desilicated HZSM-5/Al2O3 extrudates, Energy & Fuels. (2019) acs.energyfuels.9b00906. doi:10.1021/acs.energyfuels.9b00906.

[20] A. Oasmaa, D.C. Elliott, J. Korhonen, Acidity of biomass fast pyrolysis bio-oils, Energy and Fuels. 24 (2010) 6548–6554. doi:10.1021/ef100935r.

[21] S. Bezergianni, A. Dimitriadis, O. Kikhtyanin, D. Kubička, Refinery co-processing of renewable feeds, Prog. Energy Combust. Sci. 68 (2018) 29–64. doi:10.1016/j.pecs.2018.04.002.

[22] C. Wang, M. Li, Y. Fang, Coprocessing of Catalytic-Pyrolysis-Derived Bio-Oil with VGO in a Pilot-Scale FCC Riser, Ind. Eng. Chem. Res. 55 (2016) 3525–3534. doi:10.1021/acs.iecr.5b03008.

[23] A. Oasmaa, S. Czernik, Fuel oil quality of biomass pyrolysis oil - State of the art for the end users, Energy & Fuels. 13 (1999) 914–921. doi:10.1021/ef980272b.

[24] S. Czernik, A. V. Bridgwater, Overview of applications of biomass fast pyrolysis oil, Energy & Fuels. 18 (2004) 590–598. doi:10.1021/ef034067u.

[25] A. Saraeian, M.W. Nolte, B.H. Shanks, Deoxygenation of biomass pyrolysis vapors: Improving clarity on the fate of carbon, Renew. Sustain. Energy Rev. 104 (2019) 262–280. doi:10.1016/j.rser.2019.01.037.

[26] R.H. Venderbosch, A critical view on catalytic pyrolysis of biomass, ChemSusChem. 8 (2015) 1306–1316. doi:10.1002/cssc.201500115.

[27] J. Jae, G.A. Tompsett, A.J. Foster, K.D. Hammond, S.M. Auerbach, R.F. Lobo, G.W. Huber, Investigation into the shape selectivity of zeolite catalysts for biomass conversion, J. Catal. 279 (2011) 257–268. doi:10.1016/j.jcat.2011.01.019.

[28] T.R. Carlson, G.A. Tompsett, W.C. Conner, G.W. Huber, Aromatic production from catalytic fast pyrolysis of biomass-derived feedstocks, Top. Catal. 52 (2009) 241–252. doi:10.1007/s11244-008-9160-6.

[29] P.A. Horne, P.T. Williams, The effect of zeolite ZSM-5 catalyst deactivation during the upgrading of biomass-derived pyrolysis vapours, J. Anal. Appl. Pyrolysis. 34 (1995) 65–85. doi:10.1016/0165-2370(94)00875-2.

[30] J. Jae, Production of green aromatics and olefins from lignocellulosic biomass by catalytic fast pyrolysis: Chemistry, catalysis, and process development, University of Massachusetts Amherst, 2012.

[31] H. Hernando, I. Moreno, J. Fermoso, C. Ochoa-hernández, P. Pizarro, J.M. Coronado, D.P. Serrano, Biomass catalytic fast pyrolysis over hierarchical ZSM-5 and Beta zeolites modified with Mg and Zn oxides, (2017) 289–304. doi:10.1007/s13399-017-0266-6.

[32] A. Aho, A. Tokarev, P. Backman, N. Kumar, K. Eränen, M. Hupa, B. Holmbom, T. Salmi, D.Y. Murzin, Catalytic pyrolysis of pine biomass over H-beta zeolite in a dual-fluidized bed reactor: Effect of space velocity on the yield and composition of pyrolysis products, Top. Catal. 54 (2011) 941–948. doi:10.1007/s11244-011-9716-8.

[33] A. Aho, N. Kumar, K. Eränen, T. Salmi, M. Hupa, D.Y. Murzin, Catalytic Pyrolysis of Biomass in a Fluidized Bed Reactor: Influence of the Acidity of H-Beta Zeolite, Process Saf. Environ. Prot. 85 (2007) 473–480. doi:10.1205/psep07012.

[34] S.D. Stefanidis, K.G. Kalogiannis, E.F. Iliopoulou, A.A. Lappas, P.A. Pilavachi, In-situ upgrading of biomass pyrolysis vapors: Catalyst screening on a fixed bed reactor, Bioresour. Technol. 102 (2011) 8261–8267. doi:10.1016/j.biortech.2011.06.032.

[35] S. Yorgun, Y.E. Şimşek, Catalytic pyrolysis of Miscanthus × giganteus over activated alumina, Bioresour. Technol. 99 (2008) 8095–8100. doi:10.1016/j.biortech.2008.03.036.

[36] F. Ateş, M.A. Işikdağ, Influence of temperature and alumina catalyst on pyrolysis of corncob, Fuel. 88 (2009) 1991–1997. doi:10.1016/j.fuel.2009.03.008.

[37] I. Demiral, S. Şensöz, The effects of different catalysts on the pyrolysis of industrial wastes (olive and hazelnut bagasse), Bioresour. Technol. 99 (2008) 8002–8007. doi:10.1016/j.biortech.2008.03.053.

[38] M.C. Samolada, A. Papafotica, I.A. Vasalos, Catalyst Evaluation for Catalytic Biomass Pyrolysis, Energy & Fuels. 14 (2000) 1161–1167. doi:10.1021/ef000026b.

[39] P. Kim, T.G. Rials, N. Labbé, S.C. Chmely, Screening of Mixed-Metal Oxide Species for Catalytic Ex Situ Vapor-Phase Deoxygenation of Cellulose by py-GC/MS Coupled with Multivariate Analysis, Energy and Fuels. 30 (2016) 3167–3174. doi:10.1021/acs.energyfuels.6b00347.

[40] M.I. Nokkosmäki, E.T. Kuoppala, E.A. Leppämäki, A.O.I. Krause, Catalytic conversion of biomass pyrolysis vapours with zinc oxide, J. Anal. Appl. Pyrolysis. 55 (2000) 119–131. doi:10.1016/S0165-2370(99)00071-6.

[41] K.G. Kalogiannis, S.D. Stefanidis, S.A. Karakoulia, K.S. Triantafyllidis, H. Yiannoulakis, C. Michailof, A.A. Lappas, First pilot scale study of basic vs acidic catalysts in biomass pyrolysis: Deoxygenation mechanisms and catalyst deactivation, Appl. Catal. B Environ. 238 (2018) 346–357. doi:10.1016/j.apcatb.2018.07.016.

[42] S.D. Stefanidis, S.A. Karakoulia, K.G. Kalogiannis, E.F. Iliopoulou, A. Delimitis, H. Yiannoulakis, T. Zampetakis, A.A. Lappas, K.S. Triantafyllidis, Natural magnesium oxide (MgO) catalysts: A cost-effective sustainable alternative to acid zeolites for the in situ upgrading of biomass fast pyrolysis oil, Appl. Catal. B Environ. 196 (2016) 155–173. doi:10.1016/j.apcatb.2016.05.031.

[43] J. Fermoso, H. Hernando, P. Jana, I. Moreno, J. Prech, C. Ochoa-Herndndez, P. Pizarro, J.M. Coronado, J. Cejka, D.P. Serrano, Lamellar and pillared ZSM-5 zeolites modified with MgO and ZnO for catalytic fast-pyrolysis of eucalyptus woodchips, Catal. Today. 277 (2016) 171–181. doi:10.1016/j.cattod.2015.12.009.

[44] I.V. Babich, M. van der Hulst, L. Lefferts, J.A. Moulijn, P. O'Connor, K. Seshan, Catalytic pyrolysis of microalgae to high-quality liquid bio-fuels, Biomass and Bioenergy. 35 (2011) 3199–3207. doi:10.1016/j.biombioe.2011.04.043.

[45] T.S. Nguyen, L. Lefferts, K.B. Saisankargupta, K. Seshan, Catalytic Conversion of Biomass Pyrolysis Vapours over Sodium-Based Catalyst: A Study on the State of Sodium on the Catalyst, ChemCatChem. 7 (2015) 1833–1840. doi:10.1002/cctc.201500236.

[46] T.S. Nguyen, M. Zabeti, L. Lefferts, G. Brem, K. Seshan, Conversion of lignocellulosic biomass to green fuel oil over sodium based catalysts, Bioresour. Technol. 142 (2013) 353–360. doi:10.1016/j.biortech.2013.05.023.

[47] A. Imran, E.A. Bramer, K. Seshan, G. Brem, High quality bio-oil from catalytic flash pyrolysis of lignocellulosic biomass over alumina-supported sodium carbonate, Fuel Process. Technol. 127 (2014) 72–79. doi:10.1016/j.fuproc.2014.06.011.

[48] M. Zabeti, T.S. Nguyen, L. Lefferts, H.J. Heeres, K. Seshan, In situ catalytic pyrolysis of lignocellulose using alkali-modified amorphous silica alumina, Bioresour. Technol. 118 (2012) 374–381. doi:10.1016/j.biortech.2012.05.034.

[49] T.S. Nguyen, M. Zabeti, L. Lefferts, G. Brem, K. Seshan, Catalytic upgrading of biomass pyrolysis vapours using faujasite zeolite catalysts, Biomass and Bioenergy. 48 (2013) 100–110. doi:10.1016/j.biombioe.2012.10.024.

[50] T.S. Nguyen, M. Zabeti, L. Lefferts, G. Brem, K. Seshan, Conversion of lignocellulosic biomass to green fuel oil over sodium based catalysts, Bioresour. Technol. 142 (2013) 353–360. doi:10.1016/j.biortech.2013.05.023.

[51] T.S. Nguyen, T.L. Duong, T.T.T. Pham, D.T. Nguyen, P.N. Le, H.L. Nguyen, T.M. Huynh, Online catalytic deoxygenation of vapour from fast pyrolysis of Vietnamese sugarcane bagasse over sodium-based catalysts, J. Anal. Appl. Pyrolysis. 127 (2017) 436–443. doi:10.1016/j.jaap.2017.07.006.

[52] X. Xue, Z. Pan, C. Zhang, D. Wang, Y. Xie, R. Zhang, Analysis of Bio-Oil Derived from Catalytic Pyrolysis of Pine Sawdust over Sodium Salts-Supported γ-Al2O3, Environ. Prog. Sustain. Energy. (2019) 1–7. doi:10.1002/ep.13174.

[53] A. Dutta, J.A. Schaidle, D. Humbird, F.G. Baddour, A. Sahir, Conceptual Process Design and Techno-Economic Assessment of Ex Situ Catalytic Fast Pyrolysis of Biomass: A Fixed Bed Reactor Implementation Scenario for Future Feasibility, Top. Catal. 59 (2016) 2–18. doi:10.1007/s11244-015-0500-z.

[54] A. Eschenbacher, F. Goodarzi, A. Saraeian, S. Kegnæs, B.H. Shanks, A.D. Jensen, Performance of Mesoporous HZSM-5 and Silicalite-1 Coated Mesoporous HZSM-5 Catalysts for Deoxygenation of Straw Fast Pyrolysis Vapors, J. Anal. Appl. Pyrolysis. (2019) 104712. doi:10.1016/J.JAAP.2019.104712.

[55] M.W. Nolte, A. Saraeian, B.H. Shanks, Hydrodeoxygenation of cellulose pyrolysis model compounds using molybdenum oxide and low pressure hydrogen, Green Chem. 19 (2017) 3654–3664. doi:10.1039/c7gc01477e.

[56] M. Von Holle, J.R. Carpenter, D.C. Dayton, Reactive catalytic fast pyrolysis process and system, US 2019/0211268 Al, 2019. doi:10.1111/2047-8852.12112.

[57] D.C. Dayton, T. Member, A. Daniels, M. Company, Catalytic Deoxygenation of Biomass Pyrolysis Vapors to Improve Bio-oil Stability, n.d.

[58] H. Ben, A.J. Ragauskas, Heteronuclear single-quantum correlation-nuclear magnetic resonance (HSQC-NMR) fingerprint analysis of pyrolysis oils, Energy and Fuels. 25 (2011) 5791–5801. doi:10.1021/ef201376w.

[59] R.M. Happs, K. Iisa, J.R.F. Iii, Quantitative 13C NMR characterization of fast pyrolysis oils, RSC Adv. 6 (2016) 102665–102670. doi:10.1039/C6RA24044E.

[60] H. de Souza Santos, P. de Souza Santos, Pseudomorphic formation of aluminas from fibrillar pseudoboehmite, Mater. Lett. 13 (1992) 175–179. doi:10.1016/0167-577X(92)90216-7.

[61] R.S. Zhou, R.L. Snyder, Structures and transformation mechanisms of the η, γ and θ transition aluminas, Acta Crystallogr. Sect. B Struct. Sci. 47 (1991) 617–630. doi:10.1107/S0108768191002719.

[62] M. Bodaghi, A.R. Mirhabibi, H. Zolfonun, M. Tahriri, M. Karimi, Investigation of phase transition of γ-alumina to α-alumina via mechanical milling method, Phase Transitions. 81 (2008) 571–580. doi:10.1080/01411590802008012.

[63] L. Negahdar, A. Gonzalez-Quiroga, D. Otyuskaya, H.E. Toraman, L. Liu, J.T.B.H. Jastrzebski, K.M. Van Geem, G.B. Marin, J.W. Thybaut, B.M. Weckhuysen, K.M. Van Geem, Characterization and Comparison of Fast Pyrolysis Bio-oils from Pinewood, Rapeseed Cake, and Wheat Straw Using13C NMR and Comprehensive GC × GC, ACS Sustain. Chem. Eng. 4 (2016) 4974–4985. doi:10.1021/acssuschemeng.6b01329.

[64] F. Ates, S. Tophanecioglu, A.E. Putun, The evaluation of mesoporous materials as catalyst in fast pyrolysis of wheat straw, Int. J. Green Energy. 12 (2015) 57–64. doi:10.1080/15435075.2014.889005.

[65] Q. Yang, S. Wu, Wheat straw pyrolysis analysis by thermogravimetry and gas chromatography-mass spectrometry, Cellul. Chem. Technol. 43 (2009) 123–131.

[66] T.N. Pham, D. Shi, D.E. Resasco, Evaluating strategies for catalytic upgrading of pyrolysis oil in liquid phase, Appl. Catal. B Environ. 145 (2014) 10–23.

doi:10.1016/j.apcatb.2013.01.002.

[67] T.N. Pham, T. Sooknoi, S.P. Crossley, D.E. Resasco, Ketonization of Carboxylic Acids: Mechanisms, Catalysts, and Implications for Biomass Conversion, ACS Catal. 3 (2013) 2456–2473. doi:10.1021/cs400501h.

[68] R. Pestman, A. van Duijne, J.A.Z. Pieterse, V. Ponec, The formation of ketones and aldehydes from carboxylic acids, structure-activity relationship for two competitive reactions, J. Mol. Catal. A Chem. 103 (1995) 175–180. doi:10.1016/1381-1169(95)00138-7.

[69] R. Pestman, R.M. Koster, A. van Duijne, J.A.Z. Pieterse, V. Ponec, Reactions of Carboxylic Acids on Oxides, J. Catal. 168 (1997) 265–272. doi:10.1006/jcat.1997.1624.

[70] S.T. Almutairi, E.F. Kozhevnikova, I. V. Kozhevnikov, Ketonisation of acetic acid on metal oxides: Catalyst activity, stability and mechanistic insights, Appl. Catal. A Gen. 565 (2018) 135–145. doi:10.1016/j.apcata.2018.08.008.

[71] T.N. Pham, T. Sooknoi, S.P. Crossley, D. Resasco, Ketonization of carboxylic acids: Mechanism, catalysts, and implications for biomass concersion, Am. Chem. Soc. Catal. 3 (2013) 2456–2473.

[72] S. Wan, T. Pham, S. Zhang, L. Lobban, D. Resasco, R. Mallinson, Direct catalytic upgrading of biomass pyrolysis vapors by a dual function Ru/TiO_2 catalyst, AIChE J. 59 (2013) 2275–2285. doi:10.1002/aic.14038.

[73] A. Eschenbacher, P.A. Jensen, U.B. Henriksen, J. Ahrenfeldt, S. Ndoni, C. Li, J.Ø. Duus, U.V. Mentzel, A.D. Jensen, Catalytic deoxygenation of vapors obtained from ablative fast pyrolysis of wheat straw using mesoporous HZSM-5, Fuel Process. Technol. 194 (2019) 106119. doi:10.1016/J.FUPROC.2019.106119.

[74] M. Ghalibaf, T.R.K.C. Doddapaneni, R. Alén, Pyrolytic behavior of lignocellulosic-based polysaccharides, J. Therm. Anal. Calorim. 137 (2019) 121–131. doi:10.1007/s10973-018-7919-y.

[75] C. Di Blasi, A. Galgano, C. Branca, Effects of potassium hydroxide impregnation on wood pyrolysis, Energy and Fuels. 23 (2009) 1045–1054. doi:10.1021/ef800827q.

[76] N.Y. Chen, D.E. Walsh, L.R. Koenig, Fluidized Bed Upgrading of Wood Pyrolysis Liquids and Related Compounds., ACS Div. Fuel Chem. Prepr. 32 (1987) 264–275. doi:10.1021/bk-1988-0376.ch024.

[77] S.A. Channiwala, P.P. Parikh, A unified correlation for estimating HHV of solid, liquid and gaseous fuels, Fuel. 81 (2002) 1051–1063. doi:10.1016/S0016-2361(01)00131-4.

[78] F. Meshkani, M. Rezaei, Preparation of mesoporous nanocrystalline alkali promoted chromium free catalysts (Fe_2O_3–Al_2O_3–NiO) for a high temperature water gas shift reaction, RSC Adv. 5 (2015) 9955–9964. doi:10.1039/C4RA13508C.

[79] D.B. Pal, R. Chand, S.N. Upadhyay, P.K. Mishra, Performance of water gas shift reaction catalysts: A review, Renew. Sustain. Energy Rev. 93 (2018) 549–565. doi:10.1016/J.RSER.2018.05.003.

[80] J.G. Speight, Corrosion by High Acid Crude Oil, in: High Acid Crudes, Elsevier, 2014: pp.

57–75. doi:10.1016/B978-0-12-800630-6.00003-4.

[81] K. Schofield, The enigmatic mechanism of the flame ionization detector: Its overlooked implications for fossil fuel combustion modeling, Prog. Energy Combust. Sci. 34 (2008) 330–350. doi:10.1016/j.pecs.2007.08.001.

[82] R.W. Stevens, A. Shamsi, S. Carpenter, R. Siriwardane, Sorption-enhanced water gas shift reaction by sodium-promoted calcium oxides, Fuel. 89 (2010) 1280–1286. doi:10.1016/j.fuel.2009.11.035.

[83] A. Nzihou, B. Stanmore, P. Sharrock, A review of catalysts for the gasification of biomass char, with some reference to coal, Energy. 58 (2013) 305–317. doi:10.1016/j.energy.2013.05.057.